

Inclination- and dust-corrected galaxy parameters: Bulge-to-disc ratios and size-luminosity relations

Alister W. Graham^{1,2} and C. Clare Worley³

¹Centre for Astrophysics and Supercomputing, Swinburne University of Technology, Hawthorn, Victoria 3122, Australia.

²Corresponding Author: AGraham@astro.swin.edu.au

³University of Canterbury, Department of Physics and Astronomy, Private Bag 4800, Christchurch 8020, New Zealand.

Received 2008 Jan 28; Accepted 2008 May 23

ABSTRACT

While galactic bulges may contain no significant dust of their own, the dust within galaxy discs can strongly attenuate the light from their embedded bulges. Furthermore, such dust inhibits the ability of observationally-determined inclination corrections to recover intrinsic (i.e. dust free) galaxy parameters. Using the sophisticated 3D radiative transfer model of Popescu et al. and Tuffs et al., together with Driver et al.’s recent determination of the average face-on opacity in nearby disc galaxies, we provide simple equations to correct (observed) disc central surface brightnesses and scalelengths for the effects of both inclination and dust in the B, V, I, J and K passband. We then collate and homogenise various literature data sets and determine the typical intrinsic scalelengths, central surface brightnesses and magnitudes of galaxy discs as a function of morphological type. All galaxies have been carefully modelled in their respective papers with a Sérsic $R^{1/n}$ bulge plus an exponential disc. Using the bulge magnitude corrections from Driver et al., we additionally derive the average, dust-corrected, bulge-to-disc flux ratio as a function of galaxy type. With values typically less than 1/3, this places somewhat uncomfortable constraints on some current semi-analytic simulations. Typical bulge sizes, profile shapes, surface brightnesses and deprojected densities are provided. Finally, given the two-component nature of disc galaxies, we present luminosity-size and (surface brightness)-size diagrams for discs and bulges. We also show that the distribution of elliptical galaxies in the luminosity-size diagram is not linear but strongly curved.

Key words: galaxies: fundamental parameters — galaxies: photometry — galaxies: spiral — galaxies: structure — ISM: Dust, Extinction — radiative transfer

1 INTRODUCTION

Although the bulge-to-total (B/T), or bulge-to-disc (B/D), flux ratio was the third, not prime, galaxy-morphology criteria employed by Sandage (1961), its systematic behaviour along the Hubble sequence is well known (e.g. Boroson 1981; Kent 1985; Kodaira, Watanabe & Okamura 1986; Simien & de Vaucouleurs 1986). While one-third (two-thirds) of the stellar mass density in the Universe today is known to reside in bulges (discs) (e.g. Driver et al. 2007), the actual allocation of stars as a function of galaxy type is not securely known. This is however a quantity of interest. If (large) bulges, including elliptical galaxies, are the result of mergers, while discs formed via the gravitational collapse of a rotating proto-galactic cloud, or from the accretion of gas around a pre-existing galaxy, then the B/D ratio reflects the dominance of a galaxy’s formation mechanisms

(e.g. Navarro & Benz 1991; Steinmetz & Navarro 2002 and references therein). The reliable separation of bulge and disc stars is also important because of the connection between supermassive black hole mass and the physical properties of the host bulge (see the review in Ferrarese & Ford 2005).

For many years it was believed that the bulges of disc galaxies were universally described by de Vaucouleurs empirical $R^{1/4}$ model (de Vaucouleurs 1948, 1958, 1978). While deviations were occasionally noted for individual galaxies, such as the Milky Way (Kent, Dame & Fazio 1991), the above belief only began to change in earnest after Andredakis & Sanders (1994) showed that the exponential model provided a better description to the distribution of stellar light in the bulges of 34 late-type spiral galaxies; a result reaffirmed by de Jong (1996a) and Courteau, de Jong & Broeils (1996) using larger samples. However the fuller renaissance, if one can use such a term, started

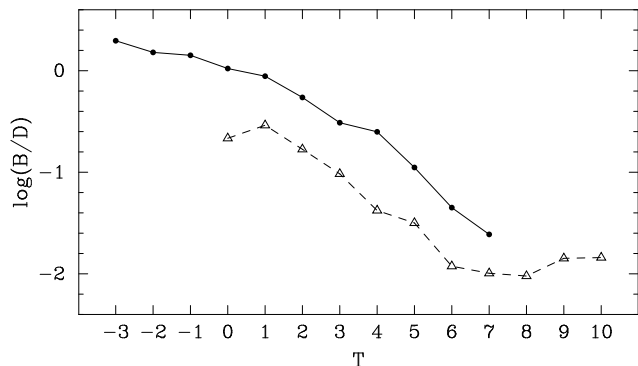


Figure 1. Average logarithm of the B -band, bulge-to-disc flux ratio as a function of galaxy morphological T -type. The solid line traces data from Simien & de Vaucouleurs (1986) who used an $R^{1/4}$ bulge + exponential disc model. The $R^{1/4}$ model is known to over-estimate the bulge flux when the bulge is better described with a Sérsic $R^{1/n}$ profile having $n < 4$ (e.g. Trujillo, Graham & Caon 2001). The dashed line traces data from Graham (2001a) who applied an $R^{1/n}$ bulge + exponential disc model to de Jong & van der Kruit’s (1994) roughly face-on ($b/a > 0.625$) sample of galaxies. Both curves, however, still need to be properly adjusted for dust attenuation.

with Andredakis, Peletier & Balcells (1995) who showed that Sérsic’s (1963, 1968) $R^{1/n}$ model was particularly well suited to describing the light-profiles of bulges. This result was subsequently confirmed by other investigations (e.g. Iodice, D’Onofrio & Capaccioli 1997, 1999; Seigar & James 1998; Khosroshahi, Wadadekar & Kembhavi 2000) and Sérsic’s model has since become the standard approach for describing bulges in both lenticular and spiral galaxies (e.g. D’Onofrio 2001; Graham 2001a; Möllenhoff & Heidt 2001; Prieto et al. 2001; Castro-Rodríguez & Garzón 2003; MacArthur et al. 2003; Balcells et al. 2007; Carollo et al. 2007).

Today, bulges are observed to follow a roughly linear magnitude-Sérsic index relation, with most bulges having Sérsic indices $n < 4$ (e.g. Graham 2001a; MacArthur et al. 2003). Indeed, Balcells et al. (2003, see their figure 1a) revealed that even lenticular galaxies typically have values of n around 2, a result which has subsequently been echoed by others (e.g. Laurikainen et al. 2006). Application of the average B/D ratios derived from studies which used $R^{1/4}$ bulge + exponential disc decomposition introduces a bias into the separation of bulge and disc flux when a bulge does not have an $R^{1/4}$ profile (e.g. de Jong 1996b; Trujillo et al. 2001; Brown et al. 2003). Specifically, given that the bulges of most disc galaxies have Sérsic indices $n < 4$, application of the $R^{1/4}$ model (with its higher central concentration of stars and greater tail at large radii) assigns too much of the galaxy flux to the bulge. Figure 1 shows the average B -band B/D ratios, as a function of galaxy type, from the data in Simien & de Vaucouleurs (1986), whose bulge magnitudes were obtained using an $R^{1/4}$ model. Also shown in Figure 1 are the B -band B/D ratios obtained by Graham (2001a) using an $R^{1/n}$ bulge model. Figure 1 is not however the end of the story, as neither study addressed the issue of attenuation of the bulge flux due to dust in the disc of the galaxies.

This brings us to our second, and often over-looked, concern. While bulges may contain little to no dust of their own — and have therefore in the past not had their flux

corrected for dust — the galaxy discs which effectively cut them in half do contain dust. Consequently, particularly at optical wavelengths, one actually sees very little of the star light from the portion of a bulge on the far side of a disc. The extent to which the bulge and disc flux is dimmed depends on both the observed wavelength and the inclination of the (dusty) stellar disc. The reduction to the observed magnitude of the bulge and disc components can be as high as 2-3 mag in the B -band (e.g. Driver et al. 2007). In spite of this, the overwhelming majority of published (optical) bulge magnitudes, and thus bulge-to-disc flux measurements, have not taken this into account and are therefore in considerable error.

On the other hand, for over the last decade most studies have corrected, at least in part, for the influence of dust on the discs. This has been accomplished by noting how parameters such as magnitude and surface brightness change with viewing angle and adjusting the observed values to those which would be observed with a face-on orientation (e.g. Valentijn 1990; de Vaucouleurs’ et al. 1991; Giovanelli et al. 1995; Tully et al. 1998; Graham 2001b; Masters et al. 2003). To obtain the intrinsic (dust-free) values of course requires an additional step: namely, correcting the face-on galaxy parameters for the influence of dust.

Sophisticated 3D dust/star galaxy models, which incorporate both clumpiness and explicit treatment of various grain compositions and sizes, now exist. The model of Popescu et al. (2000) and Tuffs et al. (2004) self-consistently explains the UV/optical/FIR/sub-mm emission from galaxies. Indeed, application of their dust model to 10,095 galaxies from the Millennium Galaxy Catalog (e.g. Allen et al. 2006) perfectly balances the amount of star light absorbed by dust in the Universe today with the amount re-radiated at infrared and sub-mm wavelengths (Driver et al. 2008). For almost a decade these models accounted for the fact that the dust is non-uniformly distributed, allowing for high extinction in the central regions, intermediate extinction in the spiral arms, and semi-transparent interarm regions which accounted for the detection of background galaxies. Their detailed model not only allows one to accurately correct for inclination-dependent extinction, but also for the additional extinction which is present when viewing galaxies with face-on orientations.

The one free parameter in their dust model which provides the calibration is the central, face-on, B -band opacity τ_B^f . Fitting a range of simulated galaxies with varying integer-values of τ_B^f , Möllenhoff, Popescu & Tuffs (2006) provided tables to correct observed disc parameters to their face-on, dust-free values. Combining their tables with the statistically determined average opacity $\tau_B^f = 3.8 \pm 0.7$ reported by Driver et al. (2007), Section 2 of this paper derives two new equations which can be used to easily correct the observed B, V, I, J and K -band disc scalelengths and central surface brightnesses for both inclination and the attenuating effect of dust, providing intrinsic, face-on, dust-free values. The above face-on, central B -band opacity from Driver et al. (2007) was obtained by matching the observed inclination-attenuation relations for the Millennium Galaxy Catalog data with the dust models of Tuffs et al. (2004).

In Section 3.1 we introduce the galaxy data sets which shall be used in our analysis of disc galaxy structural parameters, while Section 3.2 describes the methodologies adopted

to bring this data onto a uniform system. Section 4 provides tables of the mean intrinsic structural parameters as a function of galaxy type in various passbands. This encompasses disc scalelengths, central surface brightnesses and magnitudes. Average K -band bulge effective radii, effective surface brightnesses, Sérsic indices and magnitudes are also listed. In addition, and also as a function of galaxy type, we provide the median bulge-to-disc size ratio in the K -band and the median dust-corrected bulge-to-disc flux ratio in the near-infrared and various optical bands.

Finally, a selection of bivariate plots are shown in Section 5. In addition to (surface brightness)-size diagrams for discs and bulges, we provide new expressions for the size-luminosity relations of discs in early- to mid-type disc galaxies. We also present the size-luminosity relation for bulges and elliptical galaxies, emphasizing that it is not a linear relation.

While inclination corrections have been applied for many years, and are still necessary today (e.g. Bailin & Harris 2008; Maller et al. 2008; Unterborn & Ryden 2008), they only remove one of several systematic biases that cause the observed flux distribution to misrepresent the true (intrinsic) stellar distribution of galaxies. Allowances for non-homology through the use of Sérsic (bulge) models and separate dust corrections to both the disc and bulge are vital if we are to know the intrinsic physical properties of galaxies. It is hoped that the distributions and trends shown here, which have been acquired after dealing with the above three issues, as done in Driver et al. (2007), will provide valuable constraints for simulations of galaxy formation which are used to aid our understanding of galaxy evolution (e.g. Cole et al. 2006; Springel & Hernquist 2003; Almeida et al. 2008; Croft et al. 2008, and references therein).

A Hubble constant of $73 \text{ km s}^{-1} \text{ Mpc}^{-1}$ has been used when H_0 -independent distances were not available.

2 CORRECTIONS FOR DUST AND INCLINATION

2.1 Disc scalelengths and central surface brightnesses

The discs of disc galaxies contain dust, in particular various mixes of graphite and silicate. This reduces the amount of (ultraviolet, optical and near-infrared) light which escapes from such galaxies. The distribution of this dust is known not to be uniform, with the centres of discs containing more light-absorbing particles than their outskirts (Boissier et al. 2004; Popescu et al. 2005). Such dust not only decreases the observed central surface brightnesses, μ_0 , of the discs, but the radial gradients in the opacity also make the observed disc scalelengths, h , greater than their intrinsic values.

The sophisticated dust/star galaxy model of Popescu et al. (2000) and Tuffs et al. (2004) incorporates clumpiness and an explicit treatment of various grain compositions and sizes within a 3D distribution. Solving the radiative transfer equations they are able to measure the radial dependence of attenuation in various wavebands. Möllenhoff et al. (2006) has used this to provide figures and tables for the effects of varying opacity and inclination on the parameters μ_0 and h . This was done using a range of galaxy models with different integer values for the central, face-on B -band opacity τ_B^f .

Table 1. Dust correction parameters for equations 1 and 2, which have themselves been fitted to the simulated data in Figure 2. These equations can be used to correct the observed scalelengths and central surface brightnesses of discs for the effects of dust and varying inclination, reproducing the stellar distributions' intrinsic (i.e. dust-free) face-on values.

Filter	a_λ	b_λ	c_λ	d_λ
B	0.59 ± 0.06	0.44 ± 0.09	1.27 ± 0.02	0.33 ± 0.07
V	0.43 ± 0.05	0.43 ± 0.08	1.20 ± 0.02	0.39 ± 0.07
I	0.24 ± 0.04	0.46 ± 0.07	1.11 ± 0.02	0.39 ± 0.06
J	0.12 ± 0.02	0.61 ± 0.05	1.05 ± 0.01	0.28 ± 0.04
K	0.06 ± 0.01	0.79 ± 0.02	1.02 ± 0.01	0.13 ± 0.02

From a study of 10,095 nearby ($0.013 < z < 0.18$) galaxies in the Millennium Galaxy Catalogue, Driver et al. (2007) have recently constrained this mean¹ opacity to be $\tau_B^f = 3.8 \pm 0.7$. We explicitly note that this is a statistical determination of the opacity and there may well be galaxy-to-galaxy variations outside of these bounds. It should also be noted that this value does not make spiral galaxies optically thick in their outer parts or interarm regions (Popescu & Tuffs 2007). Such high central opacities are however required, or rather consistent with, the observed amount of infrared and sub-millimetre flux coming from the thermally heated dust in galaxies (Driver et al. 2008). Using the above value for the opacity, and a linear extrapolation between the gridded data points in Möllenhoff et al., the points in Figure 2 show the combined effect of dust and viewing angle (i.e. inclination) on the disc scalelength and central surface brightness² in the B, V, I, J and K passbands. The shaded region shows the range in behaviour at fixed inclination as τ_B^f changes from 3.1 to 4.5.

Using the linear regression routine FITEXY from Press et al. (1992)³ two empirical relations have been fit to the simulated data points in Figure 2. They are such that

$$\mu_{0,\text{obs}} - \mu_{0,\text{intrin}} = a_\lambda + b_\lambda [2.5 \log(\cos i)], \quad (1)$$

and

$$h_{\text{obs}}/h_{\text{intrin}} = c_\lambda - d_\lambda \log(\cos i), \quad (2)$$

for some inclination i , with $i = 0$ degrees describing a face-on orientation. To assist with the understanding of Figure 2, we note that in the absence of dust, the line-of-sight depth through a disc increases as the disc is inclined, such that the pathlength changes by $(\cos i)^{-1}$ to give $\mu_{0,\text{obs}} = \mu_{0,\text{intrin}} + 2.5 \log(\cos i)$. The parameters a_λ , b_λ , c_λ and d_λ in equations 1 and 2 are a function of wavelength, and given in Table 1. These equations can be used to correct observed values to the intrinsic face-on (dust-free) values.

¹ Possible variations of opacity with Hubble Type, and thus also luminosity, are not yet firmly established. While Driver et al. (2007) and Shao et al. (2007) did not find evidence for such a variation, this is still an open issue (e.g. Masters et al. 2003) and needs to be addressed when far-infrared and sub-mm data become available for galaxies selected from optical surveys.

² We have used columns 4 and 5 from the tables in Möllenhoff et al. (2006).

³ The uncertainty on the independent variable, namely the inclination, was set to zero. The uncertainty on the dependent variable ($\mu_{0,\text{obs}}$ or h_{obs}) arose from the uncertainty of ± 0.7 on the value $\tau_B^f = 3.8$ (Driver et al. 2007).

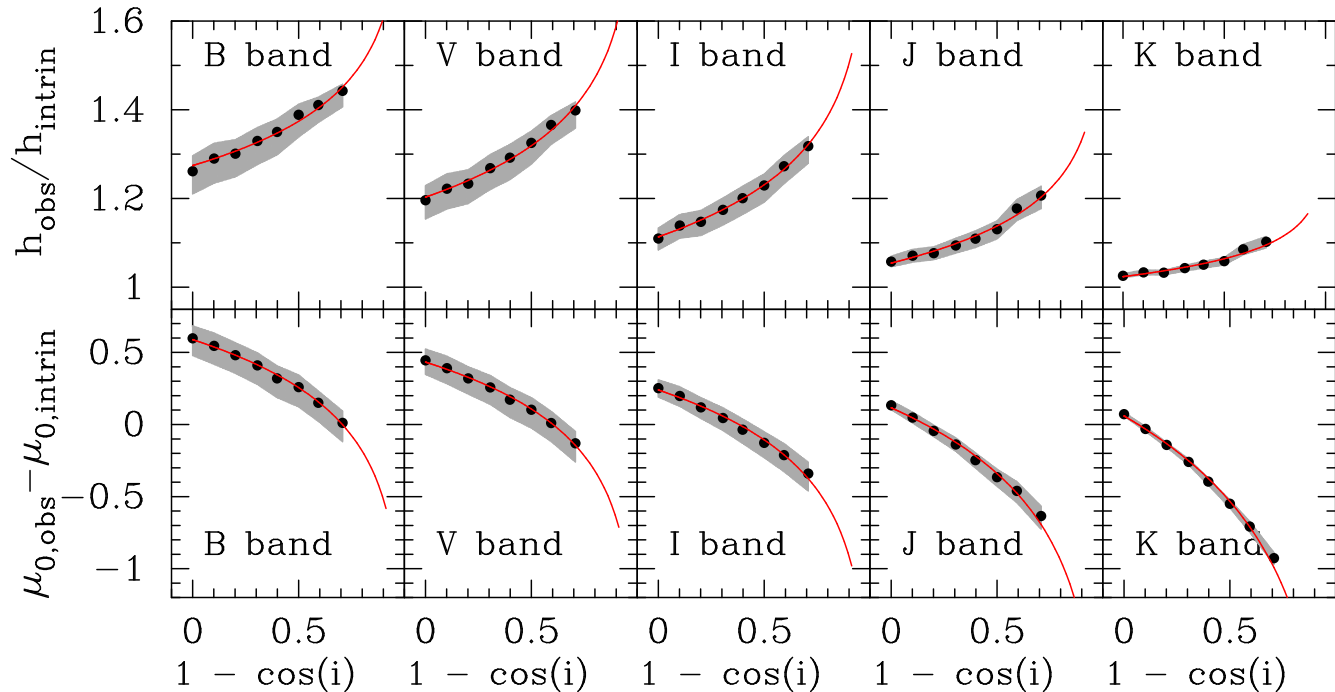


Figure 2. Inclination-attenuation corrections to the scalelength (h) and central surface brightness (μ_0) of simulated disc galaxies. The data points and the associated shaded area have been extracted from Möllenhoff et al. (2006) using the statistically determined, face-on B -band opacity $\tau_B^f = 3.8 \pm 0.7$ (Driver et al. 2007). The data points show the difference between the observed values at some inclination, i , and the intrinsic face-on ($i = 0$) values which would be observed in the absence of dust. The solid line is an empirical fit (see equations 1 and 2) using the code FITEXY from Press et al. (1992). The parameters of the fit are given in Table 1. From $0.7 < 1 - \cos i < 1.0$, the curve is an extrapolation of the model that was fitted to the data at smaller inclinations; as such it may not be applicable over this high-inclination range.

However, we caution that because the data in Möllenhoff et al. only extends to inclinations where $1 - \cos i < 0.7$, the curves shown in Figure 2 at higher inclinations are an extrapolation of these empirical models and may therefore not be reliable for systems more inclined than 73 degrees.

2.2 Bulge and disc magnitudes

In addition to the above expressions, we shall also use the equations in Driver et al. (2008) to correct the observed disc and bulge magnitudes for the effects of inclination and dust. These are given by

$$M_{\text{disc,obs}} - M_{\text{disc,intrin}} = b_1 + b_2 [1 - \cos(i)]^{b_3}, \quad (3)$$

and

$$M_{\text{bulge,obs}} - M_{\text{bulge,intrin}} = d_1 + d_2 [1 - \cos(i)]^{d_3}. \quad (4)$$

where the coefficients in the above equations depend on wavelength and are provided in Driver et al. (2008) for various passbands, including the B , r' , i' and K bands. We have used their r' and i' coefficients for our R and I band data. This approximation will not introduce any noticeable bias, as inspection of Figure 2 from Driver et al. (2008) will reveal.

The effect of dust on bulges is far more severe than generally realised. Past studies of the B/T ratio, while usually correcting the observed disc flux for inclination and dust (but typically overlooking any attenuation once adjusted to a face-on orientation), normally assume that the bulge is not affected by dust. This is wrong. Moreover,

given that bulges and discs have their own inclination-attenuation correction, which is not surprising, there is no single *galaxy* inclination-attenuation correction. That is, one must perform a bulge/disc separation. Unfortunately this may severely hamper the ability of large-scale studies (which have fitted single Sérsic models to two-component disc galaxies) to recover intrinsic galaxy parameters.

In this study we use the above formula to provide dust-corrected bulge magnitudes and dust-corrected bulge-to-disc flux ratios. However the influence of dust on the individual Sérsic parameters of the bulge (μ_e , R_e and n , see equation 5) is not well known. It will of course depend not only on the wavelength of one's observations but also on the precise star/dust geometry, with concentrated high- n bulges likely experiencing a greater degree of attenuation. Moreover, the overwhelming majority of optical bulge parameters reported in the literature are dependent, to some degree, on the happenstance inclination of their galaxy's disc. As yet unknown corrections to a dust-free configuration are required if we are to have an accurate set of physical parameters for the bulges. Nonetheless, for now, we have tabulated K -band Sérsic bulge parameters as these will be the least affected by dust.

3 THE GALAXY DATA

In this study we primarily investigate the properties of 'late-type galaxies', and more generically 'disc galaxies'. Today, the term 'early-type galaxy' is often used to refer to both

elliptical galaxies and lenticular galaxies. While the average properties of elliptical galaxies are not considered to be a function of inclination — and so one should identify and exclude such systems from current inclination-dependent analyses of the effect of dust — this is not true for systems with large scale discs. We have therefore included lenticular disc galaxies in our analysis, rather than grouping/excluding them with the elliptical galaxies in an early-type galaxy bin.

However we note that elliptical galaxies are certainly not always devoid of dust (e.g. Ebneter & Balick 1985; Sadler & Gerhard 1985; Ebneter, Djorgovski & Davis 1988; Leeuw et al. 2008). Indeed, they also frequently possess small nuclear dust lanes and dusty nuclear discs (e.g. Ferrari et al. 1999; Rest et al. 2001) which probably originate from sources such as type Ia SNe and stellar mass loss from, for example, the winds of red giant stars (Ciotti et al. 1991; Calura et al. 2008). On a galactic scale, however, the dust is destroyed rather quickly by ion sputtering from the hot X-ray gas (e.g. Temi, Brighenti & Mathews 2007). In contrast, lenticular galaxies, such as the Sombrero galaxy, are commonly observed to possess considerable amounts of dust in their discs. In this regard lenticular galaxies are more like spiral galaxies. Interestingly, Bekki, Couch & Yasuhiro (2002) and Aragón-Salamanca, Bedregal & Merrifield (2006) have argued that lenticular galaxies may be spiral galaxies in which the star formation has been turned off and the spiral pattern dispersed. If such a morphological transformation occurs, one would simultaneously require the bulge-to-disc flux ratio to increase. This may proceed via the passive fading of the disc and, as noted by Driver et al. (2008), upon removal of centrally located dust.

3.1 Literature catalogues

There has been a number of papers which have provided structural parameters for nearby disc galaxies. At the end of 2005, when selecting which of these would be suitable for our compilation of bulge and disc parameters, we applied the following criteria: (i) a Sérsic bulge model had been simultaneously fit with an exponential disc model; (ii) roughly a couple of dozen or more galaxies had been modelled; (iii) morphological (Hubble or T)⁴ types existed for the galaxies; (iv) the galaxies appeared large enough that their bulges were well-resolved (this meant that we only used studies with galaxy redshifts typically less than 0.03–0.04); (v) studies of early-type galaxies (i.e. E and S0) which had not checked if a bulge-only fit was superior to a bulge plus disc fit were excluded as many of the fitted discs (and hence the structural parameters) may be spurious; and (vi) studies in which the fitted disc frequently failed to coincide with the outer light-profile were also excluded, which included studies which often had the fitted bulge model contributing more flux than the disc model at the outer light profile. This latter problem is illustrated in Graham (2001a, his figure 7) and results in overly large Sérsic indices, B/T flux ratios

Table 2. Number of galaxies in each passband from the literature data that we were able to use. **G02** = Graham (2002), low surface brightness (LSB) galaxies only, supplemented with LSB galaxies from Graham & de Blok (2001) for which redshifts have since become available; **M04** = Möllenhoff (2004); **MCH03** = MacArthur, Courteau & Holtzman (2003); **G01** = Graham (2001a, 2003); **MH01** = Möllenhoff & Heidt (2001); **SJ98** = Seigar & James (1998); **BGP03** = Balcells, Graham & Peletier (2003); **KdJSB03** = Knapen et al. (2003); **GPP04** = Grosbøl, Patsis & Pompei (2004); **LSB05** = Laurikainen, Salo & Buta (2005); **DD06** = Dong & De Robertis (2006); **KdJP06** = Kassin, de Jong & Pogge (2006).

Study	B	V	R	I	K
G02	31	20	37	21	...
M04	25	25	24	25	...
MCH03	56	38	60
G01	74	...	72	68	74
MH01	40
SJ98	44
BGP03	19
KdJSB03	28 ^a
GPP04	53
LSB05	22 ^a
DD06	113
KdJP06	15 ^a
Total	186	83	193	114	408

^a K_s filter.

and R_e/h size ratios. This can happen when using a (signal-to-noise)-weighted bulge + disc fitting routine on a galaxy which has additional nuclear components and, as noted by Laurikainen et al. (2007) and Weinzirl et al. (2008), when significant bars are present. Our final sample selection, while almost certainly not all inclusive due to unintentionally overlooked references, is given in Table 2. Unfortunately the optical data from Hernandez-Toledo, Zendejas-Dominguez & Avila-Reese (2007) and Reese et al. (2007) appeared too late for us to include.

Individual studies meeting the above criteria contained on the order of ~ 20 to ~ 100 galaxies. Previously, when these galaxies had been binned into their morphological type (e.g. Sab, Scd, etc.), this tended to result in less than ideal numbers per bin in each of these individual studies. As a result, past answers to questions of a statistical nature, such as the typical value of, and range in, some physical parameter for a given morphological type, were poorly defined. By combining here (see Section 3.2) the data from these studies, we hope to better answer such questions. Importantly, we also apply corrections to the magnitudes of both the discs *and* the bulges (see Section 2).

We stress that while the galaxies used here are typical representations of galaxies along the Hubble sequence, we have applied no sample selection criteria to provide a magnitude-limited sample. Given the inclination-dependent reduction to magnitudes due to dust, we note in passing that such a task is not as simple as one may first think: after correcting for dust, one's original magnitude-limited sample will subsequently have a rather jagged boundary. However the desire to include as many galaxies as possible, rather than this issue, has been the driving rationale employed here.

⁴ We used de Vaucouleurs' T-type classification from the RC3 catalogue (de Vaucouleurs et al. 1991) which is roughly such that: $-3 \leq T \leq -1$ (S0), T=0 (S0/a), T=1 (Sa), T=2 (Sab) ... T=9 (Sm), T=10 (Irr).

3.2 Homogenisation

We have started with the catalogues of Sérsic-bulge and exponential-disc parameters from the studies listed in Table 2. While the exponential model used to describe the radial stellar distribution in discs has been around for a long time (e.g. Patterson 1940; de Vaucouleurs 1957; Freeman 1970), Sérsic’s (1963) 3-parameter model has only become fashionable over the last decade. It can be written as

$$\mu(R) = \mu_e + 1.086b_n \left[(R/R_e)^{1/n} - 1 \right], \quad (5)$$

where $\mu_e = -2.5 \log I_e$ is the surface brightness at the effective half-light radius R_e , and n is the Sérsic index quantifying the radial concentration of the stellar distribution. The quantity b_n is not a parameter but instead a function of n such that $\Gamma(2n) = 2\gamma(2n, b_n)$, where Γ and γ are the complete and incomplete gamma functions as given in Graham & Driver (2005). For $0.5 < n < 10$, $b_n \approx 1.9992n - 0.3271$ (Capaccioli 1989). The exponential model used to describe discs can be obtained by setting $n = 1$ in Sérsic’s model, however it is more commonly expressed as

$$\mu(R) = \mu_0 + 1.086(R/h), \quad (6)$$

in which μ_0 is the central ($R = 0$) surface brightness and h is the exponential disc scalelength.

The apparent magnitude of an exponential disc is such that

$$m_{\text{disc}} = \mu_0 - 2.5 \log(2\pi h^2), \quad (7)$$

and that of a Sérsic bulge is given by the expression

$$m_{\text{bulge}} = \mu_e - 2.5 \log(2\pi R_e^2) - 2.5 \log \left[\frac{ne^b}{b^{2n}} \Gamma(2n) \right], \quad (8)$$

with both h and R_e in arcseconds, and μ_0 and μ_e in mag arcsec⁻². The gamma function Γ has the property $2n\Gamma(2n) = \Gamma(2n + 1) = (2n)!$. Conversion from apparent magnitudes m to absolute magnitudes M proceeds via the standard expression $m - M = 25 + 5 \log(\text{Distance}[Mpc])$. Although not done here, applying one’s preferred stellar mass-to-light ratio to the absolute luminosities yields the associated stellar masses.

In practice, because we use the observed disc magnitudes, due to the apparent ellipticity ϵ of these discs — as they are seen in projection — equation 7 had the h^2 term replaced with $h^2(1 - \epsilon)$. The quantity $1 - \epsilon$ is equal to the observed minor-to-major axis ratio of the disc. As we do not have information on the ellipticity/triaxiality of the bulges, this work has assumed they are spherical (but see Méndez-Abreu et al. 2008). Unless specified in their respective papers, the inclination of each galaxy has been estimated using $\cos i = b/a$, where b/a is the *observed* outer axis ratio. Discs of course have a finite thickness, and so the applicability of this expression deteriorates when dealing with increasingly edge-on galaxies. In the past, discs have been modelled as transparent oblate spheroids (e.g. Holmberg 1946; Haynes & Giovanelli 1984; Guthrie 1992) giving rise to the relation $\cos^2 i = [(b/a)^2 - Q^2]/[1 - Q^2]$, where $Q = c/a$ is the *intrinsic* short-to-long axis ratio. Transparent edge on discs will have an ellipticity equal to Q rather than zero. Not surprisingly, the above relation breaks down in the presence of obscuring dust (Möllenhoff et al. 2006. their section 4.3 and Fig.12 which plots $[b/a]_{\text{obs}}/[\cos i]_{\text{true}}$).

The recovery of disc inclinations is not a major problem here because the majority of our galaxies have observed axis ratios $b/a > 0.34$ and therefore inclinations less than ~ 70 degrees, where the use of $\cos i = b/a$ remains a reasonable approximation. Only one galaxy (UGC 728, $b/a = 0.284$) in our optical data has b/a smaller than 0.34. In our K -band sample of over 400 galaxies, where the effect of dust on magnitudes and scalelengths are small, there are three samples with (some) discs having $b/a < 0.34$. These include (1) Dong & De Robertis (2006) where a mere six per cent of the galaxies have inclinations greater than 75 degrees and (2) Möllenhoff & Heidt (2001) from which only six galaxies have $b/a < 0.34$. As such, these few galaxies have no statistically significant impact on the results. However, for the 19 early-type disc galaxies from (3) Balcells et al. (2003), the observed ellipticities reach as high as 0.83. Unfortunately Möllenhoff et al. (2006) do not provide corrections to $\cos i$ for inclinations greater than 73 degrees, and so we have adopted the K -band value for $Q = c/a = 0.11$ which was used in the dust model of Tuffs et al. (2004).⁵ While this is not ideal, although dust is less of an issue in the K -band, we note that for the most edge-on disc galaxy, with an observed ellipticity equal to 0.83, the derived inclination changes from ~ 80 degrees to 82.5 degrees, i.e. $\cos i$ only changes from 0.17 to 0.13.

From the papers listed in Table 2 we took, when available or derivable, the five main structural parameters (μ_0, h, μ_e, R_e, n). We also took the inclination i of the disc, which, as noted above, usually came from the ellipticity ϵ of the outer isophotes such that $\epsilon = 1 - b/a = 1 - \cos i$. Potential intrinsic disc ellipticities, i.e. non-circular shapes of face-on discs (Rix & Zaritsky 1995; Andersen et al. 2001; Barnes & Sellwood 2003; Padilla & Strauss 2008), and lopsidedness (e.g. Kornreich et al. 1998; Bournaud et al. 2006; Reichard et al. 2008), have not been measured for our galaxy sample and are consequently ignored. However given the intrinsic disc ellipticity has been estimated to have a mean value of only ~ 0.05 , the uncertainty this introduces to the corrected scalelengths via equation 2 is less than 1 percent, and the uncertainty on the central surface brightnesses obtained via equation 1 is less than 0.04 mag arcsec⁻². Except in the K -band, one can see from Figure 2 that the uncertainty in the face-on opacity will introduces a greater source of scatter.

For the distances to the galaxies we consulted Tonry et al. (2001) in the case of the lenticular galaxies, and used the (Virgo + GA + Shapley) distances given in NED⁶, for the remainders. As a consequence, a Hubble constant of 73 km s⁻¹ Mpc⁻¹ has effectively been assumed. This Hubble constant is also the value reported in (Blakeslee et al. 2002) and is the halfway point between the two values reported in van Leeuwen et al. (2007).

⁵ The average B -band value of Q from Xilouris et al. (1999), which was used by Tuffs et al. (2004), is 0.074. The intrinsic stellar scaleheight reported by Xilouris et al. (1999) is largely independent of wavelength, while the intrinsic stellar scalelength decreases with wavelength. The dust model of Tuffs et al. (2004) used a K -band intrinsic stellar scalelength that was 0.683 times the B -band value, giving rise to the value 0.074/0.683 \approx 0.11.

⁶ NASA Extragalactic Database (NED, <http://nedwww.ipac.caltech.edu>).

Inclination-corrections to the disc surface brightnesses which had been applied in some papers were undone according to the prescription in each paper. The resultant ‘observed’ disc surface brightnesses were then corrected to a face-on, dust-free value using equation 1. Scalelengths — which had not been adjusted for inclination — were corrected using equation 2, and disc magnitudes were subsequently computed using equation 7.

Disc magnitudes were also derived using a second approach, in which the observed (uncorrected) magnitude was corrected using equation 3. Similarly, the observed bulge magnitudes have been corrected here using equation 4. Published Sérsic bulge parameters are not corrected for dust; expressions to do so do not exist. We therefore report on only the K -band Sérsic bulge parameters⁷ which are summarised in Table 3.

Galactic extinction corrections from Schlegel et al. (1998), as listed in NED, have been applied (if not already done so in the original paper). Cosmological redshift dimming also reduces the galaxy flux slightly, so we have applied an adjustment of $2.5 \log(1+z)^4$ to the magnitudes and surface brightnesses when not already done so. This is not a huge adjustment, for example, it amounts to 0.1 mag at a redshift corresponding to $7,000 \text{ km s}^{-1}$. Given the proximity of the galaxy samples, we have not applied evolutionary nor K -corrections.

In what follows we have grouped all S0 galaxies ($-3 \leq T \leq -1$) into a single bin, denoted by $T = -1$ in our Figures and Tables.

4 STRUCTURAL PARAMETERS AND THEIR RATIOS

4.1 The near-infrared

We have computed the median (and width of the central 68 per cent) from the distributions of various structural parameters as a function of galaxy type. In Table 3 we report the face-on, dust-free, K -band disc central surface brightness μ_0 and scalelength h , obtained using equations 1 and 2. These values of μ_0 and h have been used to derive, via equation 7, the disc magnitudes given in Table 3; they are also shown in Figure 3. Spiral galaxies are commonly referred to as ‘early’ type or ‘late’ type (Hubble 1926)⁸. Given that morphological types are not always uniquely assigned (Lahav et al. 1995), and often one only knows roughly what the actual type is, we therefore report the above parameters and ratios for the following three disc galaxy classes: lenticular galaxies (S0, S0/a); early-type spiral galaxies (Sa, Sab, Sb); and late-type spiral galaxies (Scd, Sd, Sm). To help reduce cross contamination, the Sbc and Sc types are not used in our galaxy class classification.

In Table 4 one can find the dust-corrected disc and bulge magnitudes obtained using equations 3 and 4, respectively. While equation 4 was applied to the bulge magnitudes in Table 3, equation 3 was not applied to the disc magnitudes

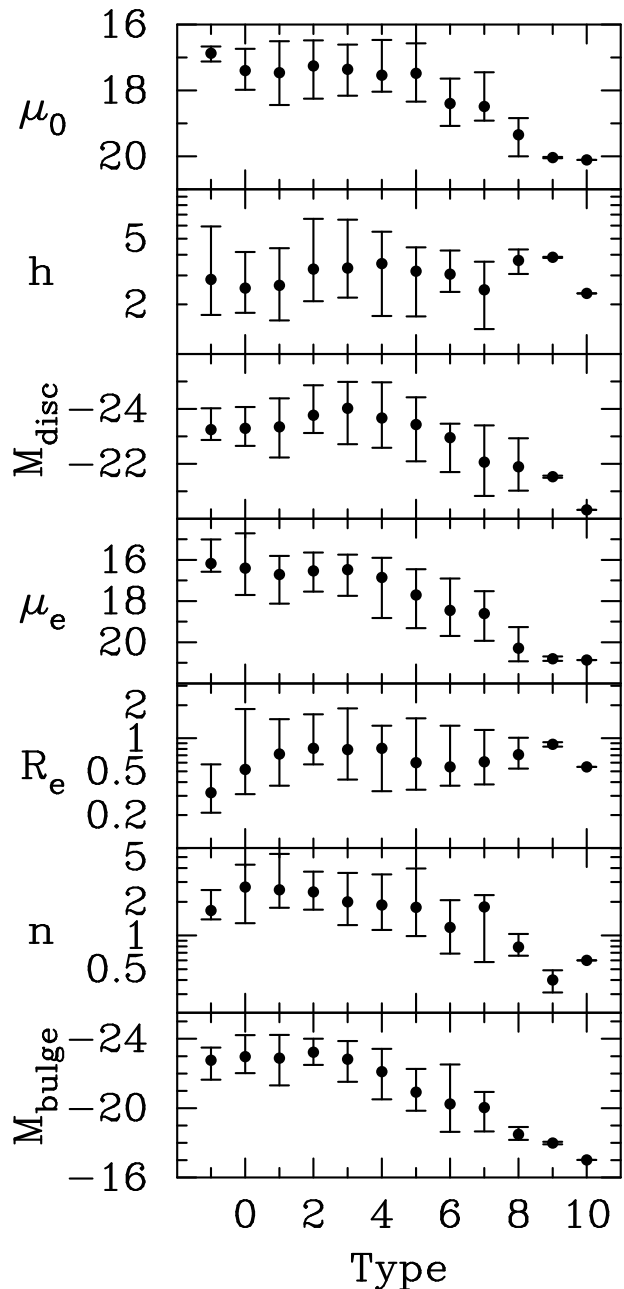


Figure 3. Standard (K -band) disc and bulge structural properties as a function of galaxy Type. For the disc, μ_0 , h and M_{disc} are the central surface brightness, scale-length and absolute magnitude. For the bulge, μ_e , R_e , n and M_{bulge} are the effective surface brightness, effective half-light radius, Sérsic index and absolute magnitude. The data have been taken from Table 3, except for the bulge magnitudes which have been taken from Table 4. For each T-Type, the median is marked with a circle and the ‘error bars’ denote the 16 and 84 per cent quartiles of the full distribution, rather than uncertainties on the median value.

from this table but the disc magnitudes obtained using the observed disc scalelengths and central surface brightnesses. Given that we now have two estimates of the corrected disc magnitude, one in Table 3 and the other in Table 4, these are compared in Figure 4 and shown to agree within a couple of tenths of a magnitude or better. A change of 0.2 mag

⁷ Differences between the K_s filter and the K -band have been ignored.

⁸ Hubble (1926) referred to Sa galaxies as early-type, Sb as intermediate, and Sc as late-type.

Table 3. *K*-band structural parameters of disc galaxies. The median, ± 34 per cent of the distribution about the median, is shown as a function of galaxy type (Column 1). Columns 2 and 3: Disc central surface brightness and scalelength corrected using equations 1 and 2, respectively. Column 4: Disc magnitude computed using equation 7 and the entries in column 2 and 3. Columns 5, 6 and 7: Observed bulge effective surface brightness, radius, and Sérsic index. Column 8: Bulge magnitude computed using equation 8 and the entries in column 5–7 (no dust correction has been applied here). Column 9: Logarithm of the bulge luminosity density $\rho_e \equiv \rho(r = R_e)L_{\odot,K} \text{pc}^{-3}$. Multiplying ρ_e by the appropriate *K*-band stellar mass-to-light ratio will give the stellar mass density at $r = R_e$ (see equation 10). The final three rows are such that $T \leq 0$ are the lenticular galaxies, $T = 1$ -3 are the early-type spiral galaxies, and $T = 6$ -9 are the late-type spiral galaxies.

Type	μ_0 mag arcsec $^{-2}$	h kpc	M_{disc} mag	μ_e mag arcsec $^{-2}$	R_e kpc	n	M_{bulge} mag	$\log \rho_e$
1	2	3	4	5	6	7	8	9
Morphological Type								
–3, –2, –1, S0	16.87 $^{+0.25}_{-0.20}$	2.83 $^{+3.10}_{-1.10}$	–23.24 $^{+0.37}_{-0.78}$	16.18 $^{+0.40}_{-1.17}$	0.32 $^{+0.26}_{-0.28}$	1.67 $^{+0.87}_{-1.58}$	–22.22 $^{+0.92}_{-0.90}$	0.78 $^{+0.27}_{-0.60}$
0, S0/a	17.40 $^{+0.58}_{-0.66}$	2.51 $^{+1.65}_{-0.73}$	–23.29 $^{+0.64}_{-0.78}$	16.40 $^{+1.31}_{-1.69}$	0.52 $^{+1.32}_{-0.21}$	2.71 $^{+1.58}_{-1.42}$	–22.58 $^{+0.67}_{-1.51}$	0.13 $^{+1.06}_{-0.89}$
1, Sa	17.46 $^{+0.98}_{-0.95}$	2.61 $^{+1.77}_{-1.01}$	–23.34 $^{+1.11}_{-1.04}$	16.71 $^{+1.42}_{-0.90}$	0.72 $^{+0.77}_{-0.35}$	2.56 $^{+2.79}_{-0.79}$	–22.67 $^{+1.52}_{-1.39}$	0.11 $^{+0.46}_{-0.85}$
2, Sab	17.26 $^{+0.99}_{-0.78}$	3.27 $^{+3.34}_{-1.18}$	–23.77 $^{+0.65}_{-1.09}$	16.54 $^{+1.00}_{-0.89}$	0.81 $^{+0.84}_{-0.23}$	2.45 $^{+1.27}_{-0.75}$	–23.11 $^{+0.95}_{-0.78}$	0.20 $^{+0.44}_{-0.77}$
3, Sb	17.36 $^{+0.80}_{-0.75}$	3.32 $^{+3.20}_{-1.12}$	–24.02 $^{+1.31}_{-0.96}$	16.48 $^{+1.27}_{-0.73}$	0.79 $^{+1.08}_{-0.37}$	2.00 $^{+1.62}_{-0.76}$	–22.59 $^{+1.29}_{-1.09}$	0.17 $^{+0.51}_{-0.75}$
4, Sbc	17.54 $^{+0.50}_{-1.07}$	3.54 $^{+1.98}_{-1.84}$	–23.67 $^{+0.99}_{-1.30}$	16.86 $^{+1.96}_{-0.96}$	0.81 $^{+0.49}_{-0.48}$	1.87 $^{+1.64}_{-0.75}$	–21.88 $^{+1.52}_{-1.34}$	0.04 $^{+0.62}_{-0.80}$
5, Sc	17.48 $^{+0.86}_{-0.91}$	3.18 $^{+1.26}_{-1.49}$	–23.43 $^{+1.34}_{-0.99}$	17.71 $^{+1.61}_{-1.25}$	0.60 $^{+0.92}_{-0.26}$	1.78 $^{+2.18}_{-0.79}$	–20.72 $^{+1.07}_{-1.41}$	–0.27 $^{+0.73}_{-0.78}$
6, Sed	18.40 $^{+0.68}_{-0.76}$	3.05 $^{+1.19}_{-0.67}$	–22.95 $^{+1.25}_{-0.51}$	18.46 $^{+1.24}_{-1.55}$	0.55 $^{+0.75}_{-0.18}$	1.18 $^{+0.89}_{-0.49}$	–20.13 $^{+1.61}_{-2.28}$	–0.43 $^{+0.79}_{-0.47}$
7, Sd	18.49 $^{+0.43}_{-1.04}$	2.45 $^{+1.18}_{-1.03}$	–22.06 $^{+1.23}_{-1.34}$	18.61 $^{+1.32}_{-1.09}$	0.61 $^{+0.58}_{-0.23}$	1.80 $^{+0.49}_{-1.22}$	–19.93 $^{+1.39}_{-0.88}$	–0.33 $^{+0.30}_{-1.06}$
8, Sdm	19.35 $^{+0.65}_{-0.51}$	3.69 $^{+0.61}_{-0.63}$	–21.89 $^{+0.87}_{-1.04}$	20.29 $^{+0.64}_{-1.02}$	0.71 $^{+0.30}_{-0.18}$	0.79 $^{+0.24}_{-0.13}$	–18.35 $^{+0.32}_{-0.43}$	–1.28 $^{+0.50}_{-0.44}$
9, Sm	20.04 $^{+0.02}_{-0.00}$	3.86 $^{+0.03}_{-0.03}$	–21.53 $^{+0.04}_{-0.04}$	20.80 $^{+0.11}_{-0.11}$	0.88 $^{+0.09}_{-0.04}$	0.40 $^{+0.09}_{-0.09}$	–17.85 $^{+0.06}_{-0.06}$	–1.61 $^{+0.06}_{-0.00}$
10, Irr	20.11 $^{+0.00}_{-0.00}$	2.33 $^{+0.00}_{-0.00}$	–20.32 $^{+0.00}_{-0.00}$	20.87 $^{+0.00}_{-0.00}$	0.55 $^{+0.00}_{-0.00}$	0.60 $^{+0.00}_{-0.00}$	–16.90 $^{+0.00}_{-0.00}$	–1.44 $^{+0.00}_{-0.00}$
Morphological Class								
–3 $\leq T \leq 0$	17.21 $^{+0.74}_{-0.49}$	2.60 $^{+1.63}_{-0.83}$	–23.27 $^{+0.60}_{-0.81}$	16.32 $^{+1.10}_{-1.51}$	0.51 $^{+1.02}_{-0.26}$	2.08 $^{+1.76}_{-0.74}$	–22.54 $^{+0.78}_{-1.47}$	0.36 $^{+0.76}_{-0.99}$
$T = 1$ -3	17.33 $^{+0.90}_{-0.84}$	3.05 $^{+2.96}_{-1.03}$	–23.73 $^{+1.21}_{-1.11}$	16.55 $^{+1.20}_{-0.87}$	0.78 $^{+0.81}_{-0.34}$	2.18 $^{+1.82}_{-0.77}$	–22.73 $^{+1.43}_{-1.18}$	0.15 $^{+0.50}_{-0.78}$
$T = 6$ -9	18.49 $^{+1.02}_{-0.87}$	3.05 $^{+1.03}_{-0.94}$	–22.58 $^{+1.59}_{-0.72}$	18.62 $^{+1.42}_{-1.73}$	0.60 $^{+0.52}_{-0.36}$	1.15 $^{+0.95}_{-0.55}$	–19.68 $^{+1.70}_{-1.43}$	–0.61 $^{+0.56}_{-0.80}$

for the disc magnitude corresponds to a change in $\log(B/D)$ of 0.08. We are also able to show such a comparison for the *B*- and *I*-band, as both sets of dust corrections are available in these bands. The slight difference in Figure 4 is thought to arise from the exponential function not providing a perfect description of dusty discs (see Möllenhoff et al. (2006, their Figure 2)). Indeed, due to the prevalence of centrally located dust, the best-fitting exponential model can be seen in Möllenhoff et al. to overestimate the observed flux at small radii. Therefore, while the corrections between the measured and intrinsic central surface brightness and disc scalelength given in equations 1 and 2 are appropriate, application of equation 7, using $\mu_{0,\text{intrinsic}}$ from equation 1, and $h_{\text{intrinsic}}$ from equation 2, can lead to a slight over-estimate of the actual observed disc magnitude. As a result, the corrections to the observed disc magnitude using this approach are not quite as large as they should be (C.Popescu & R.Tuffs 2008, priv. comm.).

4.1.1 The bulge-to-disc size ratio R_e/h

Using exponential bulge models, de Jong (1996b) suggested that the bulge-to-disc size ratio was independent of Hubble type. This unexpected result was reiterated by Courteau, de Jong & Broeils (1996) using an additional ~ 250 Sb/Sc galaxies imaged in the *r*-band. Adding to the mystery, Graham & Prieto (1999) pointed out that de Jong’s early-type spiral galaxies actually had an average R_e/h ratio — derived using his exponential bulge models — that was *smaller* (at the 3σ level in the *K*-band) than the average R_e/h ratio from his late-type spiral galaxies.

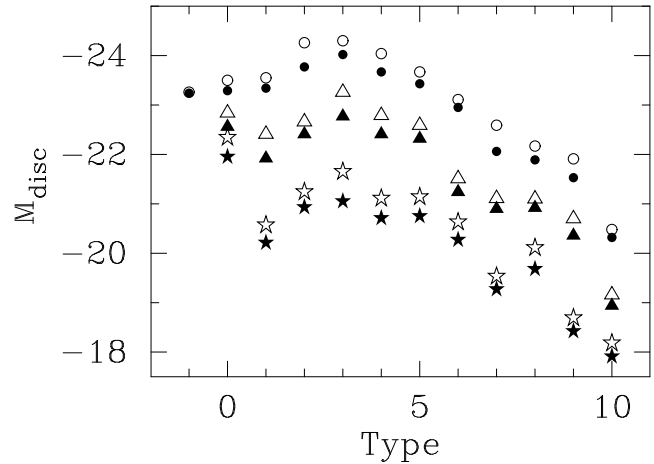


Figure 4. Comparison of our two estimates of the (corrected) disc magnitudes. The filled symbols show the median values obtained using the corrections in equations 1 and 2, while the open symbols show the median values obtained using equation 3. *B*-band: stars. *I*-band: triangles. *K*-band: circles.

Rather than only using the effective radii from de Jong’s exponential bulge models, Graham & Prieto explored use of the R_e values from de Jong’s “best-fitting” bulge model; which was either an $R^{1/4}$ model, an $R^{1/2}$ model or an exponential $R^{1/1}$ model. Doing so, the mean R_e/h ratio was shown to be slightly larger for the early-type disc galaxies than the late-type disc galaxies. Following up on this, Graham (2001a) fitted Sérsic bulge (plus exponential disc) models to all of the light profiles used by de Jong. Graham

Table 4. *K* band parameters of disc galaxies. The median, $\pm 68/2$ per cent of the distribution on either side of the median, is shown as a function of galaxy type (Column 1). Column 2: Bulge-to-disc size ratio using columns 6 and 3 from Table 3 Column 3: Bulge magnitude, obtained from the observed flux, corrected using equation 4. Column 4: Disc magnitude, obtained from the observed flux, corrected using equation 3. Column 5: Bulge-to-disc flux ratio using columns 2 and 3. Column 6: Number of data points. The bulge-to-total flux ratio can be obtained from the expression $B/T = [1 + (D/B)]^{-1}$, where B/D is the bulge-to-disc flux ratio.

Type	R_e/h	M_{bulge}	M_{disc}	$\log(B/D)$	#
Morphological Type					
-3, -2, -1, S0	$0.12^{+0.07}_{-0.04}$	$-22.76^{+1.12}_{-0.74}$	$-23.26^{+0.40}_{-1.28}$	$-0.54^{+0.28}_{-0.27}$	16
0, S0/a	$0.22^{+0.37}_{-0.09}$	$-22.97^{+0.95}_{-1.24}$	$-23.50^{+0.48}_{-0.59}$	$-0.31^{+0.46}_{-0.24}$	30
1, Sa	$0.31^{+0.20}_{-0.17}$	$-22.89^{+1.58}_{-1.34}$	$-23.55^{+1.04}_{-1.05}$	$-0.34^{+0.40}_{-0.32}$	45
2, Sab	$0.24^{+0.22}_{-0.19}$	$-23.23^{+0.73}_{-0.78}$	$-24.26^{+0.92}_{-0.92}$	$-0.54^{+0.53}_{-0.41}$	38
3, Sb	$0.21^{+0.15}_{-0.07}$	$-22.83^{+1.31}_{-1.04}$	$-24.30^{+1.15}_{-0.87}$	$-0.60^{+0.28}_{-0.39}$	60
4, Sbc	$0.21^{+0.11}_{-0.09}$	$-22.10^{+1.59}_{-1.32}$	$-24.04^{+1.14}_{-1.29}$	$-0.82^{+0.28}_{-0.42}$	79
5, Sc	$0.22^{+0.27}_{-0.09}$	$-20.92^{+1.07}_{-1.35}$	$-23.67^{+1.19}_{-1.07}$	$-1.06^{+0.43}_{-0.34}$	94
6, Scd	$0.19^{+0.10}_{-0.06}$	$-20.24^{+1.60}_{-2.28}$	$-23.11^{+1.30}_{-1.03}$	$-1.23^{+0.75}_{-0.28}$	28
7, Sd	$0.24^{+0.07}_{-0.10}$	$-20.04^{+1.38}_{-0.90}$	$-22.59^{+1.39}_{-1.04}$	$-1.06^{+0.16}_{-0.50}$	11
8, Sdm	$0.19^{+0.14}_{-0.07}$	$-18.49^{+0.32}_{-0.43}$	$-22.17^{+0.85}_{-1.07}$	$-1.49^{+0.36}_{-0.36}$	4
9, Sm	$0.23^{+0.01}_{-0.01}$	$-17.99^{+0.07}_{-0.07}$	$-21.91^{+0.10}_{-0.10}$	$-1.57^{+0.01}_{-0.01}$	2
10, Irr	$0.24^{+0.00}_{-0.00}$	$-17.01^{+0.00}_{-0.00}$	$-20.48^{+0.00}_{-0.00}$	$-1.39^{+0.00}_{-0.00}$	1
Morphological Class					
$-3 \leq T \leq 0$	$0.17^{+0.24}_{-0.08}$	$-22.96^{+1.00}_{-1.18}$	$-23.49^{+0.51}_{-0.63}$	$-0.37^{0.40}_{-0.35}$	46
$T = 1-3$	$0.24^{+0.22}_{-0.10}$	$-22.95^{+1.38}_{-1.16}$	$-24.15^{+1.15}_{-0.95}$	$-0.51^{0.45}_{-0.37}$	143
$T = 6-9$	$0.22^{+0.08}_{-0.09}$	$-19.80^{+1.72}_{-1.45}$	$-22.87^{+1.49}_{-1.14}$	$-1.19^{0.43}_{-0.40}$	45

revealed little difference between the early- and late-type disc galaxy bulge-to-disc size ratios, and therefore ultimately reached the same conclusion as Courteau et al. (1996) but on somewhat different grounds. To explain this apparent discrepancy with what one sees when looking at spiral galaxies of different type, i.e. that early-type spiral galaxies *appear* to have larger bulge-to-disc size ratios than late-type spiral galaxies, Graham (2001a, his figure 21) subsequently presented the ‘ice-berg’ model in which the intensity of the bulge varies (is effectively raised or lowered) relative to the intensity of the disc.

Using ~ 400 disc galaxies, Table 4 and Figure 5, present the *K*-band R_e/h size ratio as a function of disc galaxy type. One of the nice features of this data set is in fact its heterogeneous nature. As a result, possible biases in any one paper’s modelling are minimised and/or effectively cancelled by those from the other papers. The results shown here are therefore something of a consensus from many papers. One can see that the median value is rather stable at around $0.22^{+0.02}_{-0.03}$, with the only departure from this being (i) an increase to 0.31 for the Sa galaxies and (ii) a value of 0.12 for T-types less than zero. The first result arises from some of the shallow 2MASS data analysed by Dong & De Robertis (2006), which is responsible for the scatter to higher R_e/h , and also higher $\log B/D$, ratios than displayed by the other data. Excluding this data set, the remaining Sa galaxies have $R_e/h = 0.25$ with a variance in this distribution of 0.04. The second result above is unusual: the size ratio is equal to or less than the lower 1σ limit from every other galaxy type (not to mention that lenticular galaxies are commonly thought to have the largest bulge-to-disc ratios). This result is however again solely due to the data from one study. Modelling the bulge and bare (and disc) as separate components, Laurikainen et al. (2005) obtained these smaller ratios. In contrast, the barless galaxies from Balcells et al. (2003) with T-type less than 0 have $\langle R_e/h \rangle \sim 0.2$. From the *K*-band panel in Figure 2, one can see that uncertainties in

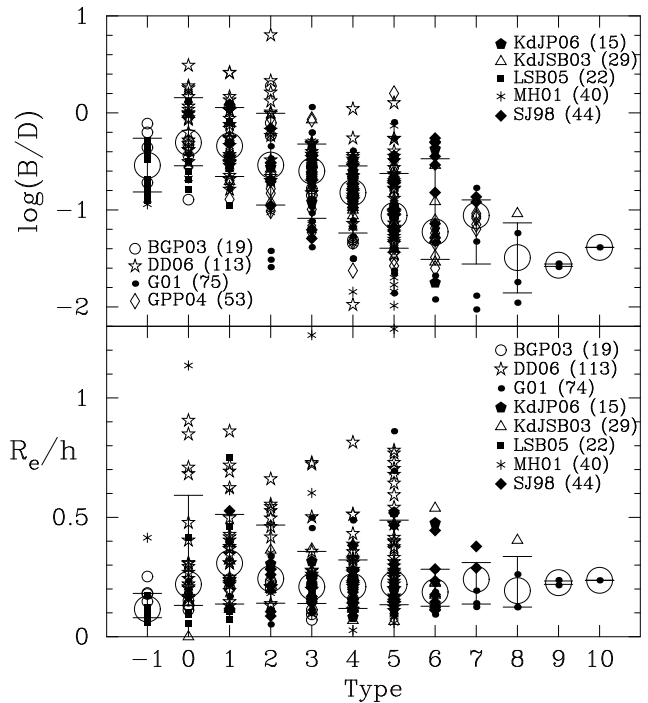


Figure 5. Top panel: *K*-band, bulge-to-disc size ratio as a function of galaxy Type. Bottom panel: Logarithm of the *K*-band, bulge-to-disc flux ratio as a function of galaxy Type. Values have been taken from Tables 4. For each Type, the median value is marked with a large circle and the ‘error bars’ denote the 16 and 84 per cent quartiles of the distribution; they thus enclose the central 68 per cent of each distribution.

the disc inclination for the Balcells et al. (2003) sample will not change this result by much.

We are unable to include the lenticular galaxies from Barway et al. (2007) as neither their fits nor bulge/disc pa-

parameters have yet been released. These authors claim that the R_e/h ratio is not (roughly) constant for all disc galaxies and that luminous lenticular galaxies can have values as high as 5 to 10, implying the presence of small embedded discs whose light peters out well before the half-light radius of the bulge component. Such potentially new objects with bulge-to-disc size ratios ~ 50 times greater than the median value of regular lenticular galaxies studied by others would surely be an important clue to the transition between disc and elliptical galaxies. If real, these discs might be more akin to the nuclear discs seen in many elliptical galaxies (e.g. Rest et al. 2001). However, we note that the sky-background should always be derived independently of one's fitted models. Barway et al.'s (undesirable) treatment of the sky-background as a free parameter when fitting the bulge and disc models may be responsible for the extreme size ratios they report. Such an approach to modelling galaxies modifies the real surface brightness profile, and may result in the occurrence of item (vi) in Section 3.1.

4.1.2 The bulge-to-disc flux ratio

The inclination- and dust-corrected K -band bulge-to-disc flux ratios, B/D , are provided in Table 4 and shown in Figure 5 as a function of galaxy type. Unlike the size ratio, the flux ratio does indeed decrease with increasing galaxy type. The early-type spiral galaxies (Sa-Sb) have a median value of $\log(B/D) = -0.49$ (i.e. $B/D = 0.32$, or equivalently a bulge-to-total flux ratio $B/T = 0.24$), where B and D represent the luminosity (not magnitude) of the bulge and disc respectively. The late-type spiral galaxies (Scd-Sm) have a median value of $\log(B/D) = -1.40$ ($B/D = 0.04$, $B/T = 0.04$).

The tabulated K -band B/D flux ratios for the 12 lenticular galaxies in Andredakis et al. (1995, their table 4) give a mean B/T ratio of 0.28. Similarly, as reported in Balcells et al. (2007), the mean (plus or minus the standard deviation) of the B/T flux ratio for the lenticular galaxies analysed in Balcells et al. (2003) is $0.25 (\pm 0.09)$. Laurikainen et al. (2005) also obtained a similar result from their K -band data, reporting a mean value of $0.24 (\pm 0.11)$ from a sample of 14 S0 galaxies while the data in Gadotti (2008) yields an R -band value of 0.28 from their 7 lenticular galaxies. Our result implies that $(50+68/2=)$ 84 percent of lenticular galaxies have B/T ratios smaller than $\sim 1/3$. The remark in Kormendy (2008) that “almost no pseudobulges have $B/T > 1/3$ ” could thus be expanded to read “most disc galaxies have $B/T < 1/3$ ”.

The above ratios, obtained from the collective average of nine modern studies (see Table 2), are smaller than those reported in the 1980s. Indeed, many late-type spiral galaxies have bulge fluxes which are less than 4 per cent of their galaxy's total light. While Shields et al. (2008) claim that the T=6 (Scd) galaxy NGC 1042 may be a bulgeless galaxy, its optical light profile in Böker et al. (2003, their Figure 1)⁹ together with its K -band light profile in Knapen

et al. (2003), plus the diffuse glow of central light in the optical images, reveals an excess of flux over the inner 2 kpc which is well above that defined by the inward extrapolation of the outer exponential light profile. Our corrected K -band bulge magnitude (and B/T ratio) for MGC 1042 is -19.13 mag (0.054), implying a supermassive black hole mass of $3 \times 10^6 M_\odot$ (Graham 2007), in agreement with the upper bound estimated by Shields et al. (2008). We therefore caution that it can be difficult when determining if a galaxy is actually bulgeless, which is a topic of particular interest at the low-mass end of relations involving supermassive black hole masses (e.g. Satyapal et al. 2007, 2008). It is not yet determined if massive black can holes form (at any redshift) before or without a host bulge. Local galaxies may shed insight into this ‘chicken-egg’ problem of whether the bulge or black hole formed first, if not in tandem.

Laurikainen et al. (2007, their figure 1) recently presented a set of K - and H -band B/T flux ratios versus galaxy type for a sample of lenticular galaxies and the spiral galaxies from the Ohio State University Bright Galaxy Survey (Eskridge et al. 2002). Although that data has not been fully corrected for dust attenuation — which is not insignificant in the H -band (e.g. Peletier & Willner 1992; Driver et al. 2008) — the trend which they show embodies the general behaviour observed here. In a separate study, Dong & De Robertis (2006) claim that their K -band flux ratio versus galaxy type diagram (their fig.7) agrees with the original B -band results given by Simien & de Vaucouleurs (1986). While roughly true, such an agreement should not occur given the differing bulge and disc stellar populations (and hence colours in the B - and K -band) for late-type disc galaxies. Aside from this problem, much of the agreement arises from the partial cancellation of two significant errors: Simien & de Vaucouleurs over-estimated their bulge flux due to the use of $R^{1/4}$ models while at the same time they neglected the dimming effects of dust. Working with $R^{1/n}$ -bulge models in the K -band, Dong & De Robertis (2006) overcame these issues.

Recent claims that the luminosity of the bulge, rather than the B/D ratio, is the driving force behind the trend seen in Figure 5 (e.g. Trujillo et al. 2002; Scannapieco & Tissera 2003; Balcells et al. 2007) reflect the results in Yoshizawa & Wakamatsu (1975, their figures 1 and 2) and echo the remarks in Ostriker (1977) and Meisels & Ostriker (1984) that the bulge luminosity, and ergo mass, may be a key parameter which distinguishes galaxies. In Figure 3 we show, separately, the bulge and disc magnitude as a function of galaxy T-type. One can see that the disc magnitude is roughly constant from T= -1 to T= 4 and then it falls by a couple of magnitude upon reaching T= 9 (Sdm galaxy). On the other hand, the bulge magnitude is roughly constant from T= -1 to T= 3, but then falls five magnitude by T= 9. We therefore confirm that the bulge magnitude is indeed predominantly responsible for the trend between the bulge-to-disc luminosity and disc galaxy type. In passing we note that Hernandez & Cervantes-Sodi (2006) have advocated that the spin parameter is the physical quantity which determines a disc galaxy's Hubble Type (see also Foyle et al. 2008); implying that the spin parameter must therefore be connected with the magnitude of the bulge.

Simien & de Vaucouleurs (1986) presented a Figure showing the mean difference between the bulge and galaxy

⁹ The bump in Böker et al.'s (2003) optical light profile for NGC 1042 at 4 ± 2 kpc is due to prominent inner spiral arms which cause a clear excess above the disc's underlying exponential light profile.

magnitude as a function of morphological T-type. Also shown in their Figure was the associated statistical uncertainty on their mean differences, which is of course much smaller than the actual scatter about each mean. They fitted a quadratic relation to this δM -T data, which has been popular in semi-analytical studies in which bulge-to-disc ratios are known but little information about the spiral arms is available. Although one could fit a relation to the median B/D ratios as a function of T-type in Figure 5, we feel that this may be misleading. For example, if $\log(B/D) = -0.5$, the actual T-type could range from -1 (S0) to 6 (Scd), while an equation would give only one value. The range of values reminds us that the bulge-to-disc flux ratio was never used as the primary criteria for classifying disc galaxy morphology. However, given the prominence of a bulge reflects the relative dominance of certain construction processes, which may be different to those which generate spiral patterns, then it may at times be desirable to employ such quantitative measures without recourse to Hubble type.

Knowing the stellar mass-to-light ratio of the bulge and disc components allows one to transform the bulge-to-total flux ratios, B/T , into stellar mass ratios. This aids comparison with cosmological simulations of galaxies. The stellar bulge-to-total mass ratio is given by $\{1 + \chi[(B/T)^{-1} - 1]\}^{-1}$, where $\chi = (M/L)_{\text{disc}}/(M/L)_{\text{bulge}}$ is the ratio of the disc and bulge stellar mass-to-light ratios, and B/T is of course the bulge-to-total flux ratio. If we use a slightly extreme (low) value of $\chi = 1/2$ (see Bruzual & Charlot 2003), then for $B/T = 0.25$ (0.33) we have a bulge-to-total stellar mass ratio of 0.4 (0.5).

To date, most simulations have a tendency to produce bulges rather than (pure) discs because of baryon angular momentum losses during merger events (Navarro & Benz 1991; Navarro & White 1994; van den Bosch 2001; D’Onghia et al. 2006). To avoid this issue, while still maintaining the hierarchical merger trees for CDM halos, potentially unrealistic amounts of feedback have been invoked in the past. Early feedback could blow much of the baryons out of high- z galaxy discs for their late-time, and necessarily post major-merger, re-accretion into some preferred plane and thereby produce the disc-dominated galaxies observed in the local Universe (see Abadi et al. 2003a). From the ~ 1000 spiral galaxies simulated by Croft et al. (2008), at $z = 1$ only 3.5 per cent have a bulge-to-total stellar mass ratio smaller than 0.5. Given that 68 per cent of real lenticular galaxies have B/T smaller than $\sim 1/3$, these simulations are clearly inconsistent with what is observed in the Universe. The disc galaxy simulated by Abadi (2003b) has a stellar bulge-to-total mass ratio of 0.71, and as such it also does not represent a typical disc galaxy. While the high mass and force resolution Λ CDM simulated spiral galaxy in Governato et al. (2004) has $B/T = 0.26$, subsequent high-resolution simulations (e.g. D’Onghia et al. 2006) reveal that resolution issues are not the key problem but rather some primary physics may still be missing. Current implementation of supernovae feedback, for example, has been shown to play a significant role in the evolution of simulated galaxies (Okamoto et al. 2005; Governato et al. 2007; Scannapieco et al. 2008 and references therein).

The current data may hopefully help determine how bulges should be assigned their mass in semi-analytical models. Such studies build galaxies by a trial and error process

in which the model assumptions, parameters and processes are collectively tweaked until the simulations resemble real galaxies. For example, when a simulated disc becomes unstable (Mo et al. 1998; Cole et al. 2000), Croton et al. (2006, their equation 22) transfer enough disc mass to the bulge in order to maintain stability, while Bower et al. (2006, their equation 1) transform the entire system into an elliptical galaxy. In the case of minor mergers (mass ratio < 0.3), some works assign all the accreted gas to the disc while transferring all the accreted stars to the bulge (de Lucia et al. 2006), while others add both the stars and cold gas to the disc of the primary galaxy (Kauffmann & Haehnelt 2000). The new bulge-to-disc flux ratio data may help to refine how these semi-analytical models operate.

4.1.3 Bulge profile shape

Although equations to correct the Sérsic parameters pertaining to the bulge are not yet available, we note that the influence of dust at wavelengths around 2 microns is noticeably less than in the optical bands (e.g. Whitford 1958; Cardelli, Clayton & Mathis 1989; Fitzpatrick 1999). The significant change to $\mu_{0,K}$ with inclination which is seen in Figure 2 is not because of dust but predominantly due to the greater line-of-sight depth through the (near-transparent) disc with increasing disc inclination. In the absence of dust, a spherical bulge will look the same from all angles, i.e. inclinations. We therefore do not expect the K -band bulge parameters to change greatly (i.e. more than a few tenths of a magnitude, or ~ 20 per cent in size) with inclination, and we report their observed values in Table 3.

As can be seen in Figure 3, Sc galaxies and earlier types typically have values of $n \sim 2$ and sometimes as high as 4. While Scd galaxies and later types tend to have values of $n < 2$, some Sd galaxies can still have values of n greater than 2. It may therefore be misleading to label all Sc and later-type galaxies as possessing pseudobulges built from exponential discs (Erwin et al. 2003; Kormendy & Kennicutt 2004, their section 4.2; Athanassoula 2008). While a value of $n = 1$ in Sérsic’s model describes an exponential profile, it does necessitate the presence of a flattened, rotating, exponential disc rather than a spheroidal, pressure supported bulge. Dwarf elliptical galaxies also have values of $n < 2$ (e.g. Caon et al. 1993; Young & Currie 1994; Jerjen et al. 2000) — they define the low-mass end of a linear relation between magnitude and Sérsic index (e.g. Graham et al. 2006b, their figure 1; Nipoti, Londrillo & Ciotti 2006). Dwarf ellipticals, however, are generally not considered to have formed from the secular evolution of a disc.¹⁰ Subsequently, disc galaxy bulges with values of $n < 2$ (or $n \sim 1$) are not necessarily pseudobulges and should not be (re-)classified as such based on this criteria alone. To clarify Kormendy & Kennicutt (2004), while pseudobulges may have $n \sim 1$, a bulge with $n \sim 1$ need not be a pseudobulge.

Although not a new result, the preponderance of bulges with $n < 4$ combined with the prevalence of late-type disc

¹⁰ Note: even if dwarf elliptical galaxies had formed from the violent redistribution of a disc, they need not preserve the disc’s exponential radial profile shape.

galaxies having bulges with $n \sim 1$ necessitates that simulations of disc galaxies neither use nor create an $R^{1/4}$ -like bulge for every galaxy. While the projection of Hernquist’s (1990) useful model — employed in many numerical simulations (e.g. Springel et al. 2005b; Di Matteo et al. 2005) — reproduces an $R^{1/4}$ profile, it does not provide a particularly good representation of bulges, such as the Milky Way’s bulge, which have $n \sim 1$ (e.g. Terzić & Graham 2005, their Figure 7; Terzić & Sprague 2007). Furthermore, efforts to simulate a range of disc galaxies with different morphological types by only varying the bulge-to-disc mass ratio, but using a Hernquist model for every bulge (e.g. Springel et al. 2005a), i.e. effectively assigning a de Vaucouleurs profile to every bulge, will not generate a realistic set of galaxies. In the case of bulges formed from disc instabilities, one requires the production of bulges that have exponential light profiles rather than Hernquist-like density profiles. In regard to simulations of minor mergers, in which bulges are built up within discs, the observed correlation between bulge profile shape and luminosity, and also supermassive black hole mass (Graham & Driver 2007), must be reproduced. The recovery of bulge parameters using $R^{1/4}$ -based models is known to introduce systematic biases with profile shape and thus also black hole mass (e.g. Trujillo et al. 2001, their Figures 4 and 5; Brown et al. 2003, their Figure 7). Therefore, once realistic bulges are generated, the computation of their sizes and binding energy by assuming a Hernquist model would be inappropriate and lead to spurious correlations when constructing, for example, a black hole fundamental plane (Younger et al. 2008).

Density models such as that from Einasto (1965) and Prugniel & Simien (1997) contain a “shape parameter” that effectively captures the range of structural shapes (Sérsic indices) which real bulges are observed to possess.¹¹ Such models have already provided insight into the gravitational torques which oblate and triaxial bulges generate. Interestingly, it is bulges with smaller Sérsic indices which have a greater non-axisymmetric gravitational field: this is because bulges increasingly resemble central point sources as the Sérsic index increases (Trujillo et al. 2002).

By construction, the three-parameter (ρ_e, R_e, n) density model of Prugniel & Simien (1997; their equation B6) contains two identical parameters to Sérsic’s model and can be written as

$$\rho(r) = \rho_e \left(\frac{r}{R_e} \right)^{-p} e^{-b[(r/R_e)^{1/n} - 1]}, \quad (9)$$

$$\rho_e = \frac{M}{L} \frac{I_e}{R_e} \frac{b^n(1-p) \Gamma(2n)}{2\Gamma(n(3-p))}, \quad (10)$$

where r is the internal, i.e. not projected, radius (see Márquez et al. 2001; Terzić & Graham 2005, their equation 4). For clarity, the subscript n has been dropped from the term b_n . The new parameter ρ_e is the internal density at $r = R_e$ and provides the normalisation such that the total mass from equation (9) equals that obtained from

¹¹ Kinematical expressions associated with these models, plus equations to convert projected densities such as $\langle \mu \rangle_e$ into three-dimensional densities, are given in Terzić & Graham (2005), Merritt et al. (2006) and Graham et al. (2006a).

Table 6. V band parameters. The median, $\pm 68/2$ per cent of the distribution on either side of the median, is shown as a function of galaxy type (Column 1). Columns 2 and 3: Face-on, disc central surface brightness and scalelength corrected using equations 1 and 2, respectively. Column 4: Disc magnitude computed using equation 7 and the entries in column 2 and 3. Column 5: Number of data points.

Type	μ_0	h	M_{disc}	#
1	2	3	4	5
Morphological Type				
−3, −2, −1, S0	0
0, S0/a	21.08 ^{+0.00} _{−0.00}	9.91 ^{+0.00} _{−0.00}	−22.70 ^{+0.00} _{−0.00}	1
1, Sa	20.15 ^{+1.57} _{−0.06}	3.15 ^{+5.75} _{−0.62}	−20.94 ^{+0.82} _{−1.16}	7
2, Sab	20.44 ^{+0.41} _{−1.11}	4.12 ^{+2.90} _{−1.76}	−21.29 ^{+0.62} _{−0.68}	5
3, Sb	19.90 ^{+0.57} _{−0.43}	4.20 ^{+2.21} _{−1.35}	−21.50 ^{+0.49} _{−0.88}	19
4, Sbc	20.04 ^{+0.47} _{−1.06}	3.78 ^{+2.29} _{−2.26}	−21.26 ^{+0.80} _{−0.55}	15
5, Sc	19.78 ^{+0.56} _{−0.19}	3.10 ^{+1.05} _{−0.48}	−21.45 ^{+0.96} _{−0.26}	20
6, Scd	20.03 ^{+0.58} _{−0.80}	3.24 ^{+0.44} _{−2.01}	−20.72 ^{+0.98} _{−0.51}	9
7, Sd	21.75 ^{+0.14} _{−0.89}	3.58 ^{+1.24} _{−0.65}	−19.52 ^{+0.24} _{−1.60}	5
8, Sdm	21.13 ^{+0.25} _{−0.25}	2.74 ^{+0.81} _{−0.81}	−21.14 ^{+0.70} _{−0.70}	2
9, Sm				0
10, Irr				0
Morphological Class				
−3 ≤ T ≤ 0	21.08 ^{+0.00} _{−0.00}	9.91 ^{+0.00} _{−0.00}	−22.70 ^{+0.00} _{−0.00}	1
$T = 1-3$	20.09 ^{+0.93} _{−0.63}	3.83 ^{+3.90} _{−1.36}	−21.49 ^{+0.76} _{−0.86}	31
$T = 6-9$	20.59 ^{+1.06} _{−1.34}	3.34 ^{+0.97} _{−1.69}	−20.68 ^{+1.25} _{−1.14}	16

equation (5) after applying the appropriate stellar mass-to-luminosity ratio M/L . Equation (10) has the same functional form as Sérsic’s model although multiplied by an additional power-law term with exponent $p = p(n)$. We adopt Lima Neto et al.’s (1999) expression for p , for which a high-quality match between deprojected Sérsic profiles and the above expression is obtained when $p = 1.0 - 0.6097/n + 0.05563/n^2$.

After converting the observed K -band bulge effective radii into units of parsecs, and the observed K -band effective surface brightnesses into units of absolute solar luminosity per square parsec, we have used equation (10) to derive the mean $\rho_e/(M/L)$ values for bulges of each galaxy type and class. These luminosity densities are provided in Table 3. To do this we used an absolute K -band magnitude for the Sun of 3.33 mag (Cox 2000). Multiplying by one’s preferred stellar M/L ratio gives the stellar mass density of the bulge at $r = R_e$. The mean R_e , n and ρ_e values can be used to construct realistic bulges using the Prugniel-Simien model, and/or to test if simulated bulges match the typical density profiles of real galaxy bulges.

4.2 The optical

As with the K -band data, we have collated literature data on the structural parameters of galaxies measured at optical wavelengths (see Table 2). After first removing any inclination corrections applied in these papers, we again employed equations 1 and 2 to determine the disc central surface brightnesses and scalelengths, and we computed the disc magnitudes using equation 7. The results are shown in Tables 5 to 8.

While dust is expected to modify the individual bulge Sérsic parameters at optical wavelengths — and for this reason we don’t present such values here — we can apply the

Table 5. *B* band parameters. The median, $\pm 68/2$ per cent of the distribution on either side of the median, is shown as a function of galaxy type (Column 1). Columns 2 and 3: Face-on, disc central surface brightness and scalelength corrected using equations 1 and 2, respectively. Column 4: Disc magnitude computed using equation 7 and the entries in columns 2 and 3. Column 5: Bulge magnitude, obtained from the observed flux, corrected using equation 4. Column 6: Disc magnitude, obtained from the observed flux, corrected using equation 3. Column 7: Bulge-to-disc flux ratio using columns 5 and 6. Column 8: Number of data points.

Type	μ_0	h	M_{disc}	M_{bulge}	M_{disc}	$\log(B/D)$	#
1	2	3	4	5	6	7	8
Morphological Type							
-3, -2, -1,S0	0
0, S0/a	21.48 ^{+0.32} _{-0.47}	6.54 ^{+3.47} _{-2.49}	-21.95 ^{+1.72} _{-0.15}	-20.81 ^{+1.16} _{-0.41}	-22.34 ^{+1.81} _{-0.16}	-0.46 ^{+0.16} _{-0.10}	3
1, Sa	20.95 ^{+0.38} _{-0.18}	3.00 ^{+6.70} _{-0.85}	-20.21 ^{+0.94} _{-1.40}	-20.08 ^{+2.06} _{-0.99}	-20.57 ^{+0.76} _{-1.56}	-0.29 ^{+0.43} _{-0.41}	9
2, Sab	20.89 ^{+0.95} _{-0.64}	5.05 ^{+5.10} _{-2.57}	-20.93 ^{+0.83} _{-0.97}	-20.38 ^{+1.22} _{-1.23}	-21.24 ^{+0.75} _{-1.20}	-0.39 ^{+0.27} _{-0.51}	10
3, Sb	20.77 ^{+0.81} _{-0.56}	3.68 ^{+4.29} _{-1.77}	-21.05 ^{+1.45} _{-0.80}	-19.50 ^{+2.16} _{-1.02}	-21.65 ^{+1.51} _{-0.84}	-0.87 ^{+0.44} _{-0.42}	32
4, Sbc	20.72 ^{+0.57} _{-0.66}	3.86 ^{+2.88} _{-1.98}	-20.71 ^{+1.14} _{-0.87}	-17.76 ^{+1.40} _{-2.26}	-21.11 ^{+1.00} _{-0.91}	-1.13 ^{+0.42} _{-0.51}	40
5, Sc	20.60 ^{+0.65} _{-0.70}	3.37 ^{+1.66} _{-0.88}	-20.75 ^{+0.66} _{-0.46}	-18.04 ^{+1.32} _{-1.11}	-21.14 ^{+0.68} _{-0.50}	-1.28 ^{+0.46} _{-0.24}	49
6, Scd	21.23 ^{+0.53} _{-1.26}	3.36 ^{+1.56} _{-1.17}	-20.27 ^{+1.40} _{-0.43}	-16.41 ^{+0.63} _{-1.47}	-20.63 ^{+1.43} _{-0.44}	-1.55 ^{+0.30} _{-0.30}	16
7, Sd	22.10 ^{+0.86} _{-0.49}	3.32 ^{+1.80} _{-0.83}	-19.27 ^{+0.92} _{-1.21}	-16.24 ^{+1.70} _{-1.02}	-19.53 ^{+0.80} _{-1.29}	-1.55 ^{+0.56} _{-0.39}	13
8, Sdm	21.74 ^{+0.76} _{-0.22}	3.88 ^{+1.08} _{-1.58}	-19.68 ^{+1.43} _{-0.30}	-15.88 ^{+1.36} _{-0.66}	-20.11 ^{+1.41} _{-0.27}	-1.69 ^{+0.53} _{-0.24}	6
9, Sm	22.61 ^{+0.75} _{-0.46}	3.72 ^{+0.71} _{-1.37}	-18.42 ^{+0.66} _{-0.88}	-15.33 ^{+1.23} _{-0.37}	-18.69 ^{+0.51} _{-1.10}	-1.53 ^{+0.16} _{-0.14}	7
10, Irr	22.25 ^{+0.00} _{-0.00}	2.06 ^{+0.00} _{-0.00}	-17.91 ^{+0.00} _{-0.00}	-14.27 ^{+0.00} _{-0.00}	-18.18 ^{+0.00} _{-0.00}	-1.57 ^{+0.00} _{-0.00}	1
Morphological Class							
-3 $\leq T \leq$ 0	21.48 ^{+0.32} _{-0.47}	6.54 ^{+3.47} _{-2.49}	-21.95 ^{+1.72} _{-0.15}	-20.81 ^{+1.16} _{-0.41}	-22.34 ^{+1.81} _{-0.16}	-0.46 ^{+0.16} _{-0.10}	3
$T = 1-3$	20.80 ^{+1.13} _{-0.57}	3.76 ^{+5.69} _{-1.84}	-20.87 ^{+1.32} _{-0.97}	-19.61 ^{+1.76} _{-1.26}	-21.34 ^{+1.31} _{-1.07}	-0.71 ^{+0.59} _{-0.50}	51
$T = 6-9$	21.77 ^{+0.96} _{-1.12}	3.67 ^{+1.18} _{-1.71}	-19.47 ^{+1.23} _{-1.18}	-15.93 ^{+1.42} _{-1.55}	-19.83 ^{+1.22} _{-1.14}	-1.58 ^{+0.38} _{-0.32}	42

Table 8. *I* band parameters. The median, $\pm 68/2$ per cent of the distribution on either side of the median, is shown as a function of galaxy type (Column 1). Columns 2 and 3: Face-on, disc central surface brightness and scalelength corrected using equations 1 and 2, respectively. Column 4: Disc magnitude computed using equation 7 and the entries in columns 2 and 3. Column 5: Bulge magnitude, obtained from the observed flux, corrected using equation 4. Column 6: Disc magnitude, obtained from the observed flux, corrected using equation 3. Column 7: Bulge-to-disc flux ratio using columns 5 and 6. Column 8: Number of data points.

Type	μ_0	h	M_{disc}	M_{bulge}	M_{disc}	$\log(B/D)$	#
1	2	3	4	5	6	7	8
Morphological Type							
-3, -2, -1,S0	0
0, S0/a	20.17 ^{+0.37} _{-0.37}	7.63 ^{+2.84} _{-2.84}	-22.56 ^{+0.60} _{-0.60}	-22.31 ^{+0.89} _{-0.89}	-22.84 ^{+0.65} _{-0.65}	-0.21 ^{+0.09} _{-0.09}	2
1, Sa	19.49 ^{+0.83} _{-1.03}	3.43 ^{+5.07} _{-1.37}	-21.92 ^{+0.77} _{-1.09}	-22.49 ^{+2.40} _{-1.04}	-22.41 ^{+0.83} _{-0.99}	-0.24 ^{+0.42} _{-0.30}	9
2, Sab	19.42 ^{+0.80} _{-0.80}	5.32 ^{+1.37} _{-3.32}	-22.41 ^{+1.02} _{-0.88}	-22.15 ^{+1.04} _{-0.93}	-22.66 ^{+0.99} _{-0.98}	-0.16 ^{+0.28} _{-0.68}	8
3, Sb	19.07 ^{+0.24} _{-0.90}	3.85 ^{+3.02} _{-1.98}	-22.77 ^{+1.51} _{-0.51}	-21.62 ^{+1.64} _{-1.00}	-23.26 ^{+1.76} _{-0.43}	-0.53 ^{+0.27} _{-0.30}	16
4, Sbc	19.28 ^{+0.40} _{-1.10}	4.41 ^{+2.73} _{-2.95}	-22.41 ^{+1.20} _{-1.01}	-20.74 ^{+1.84} _{-1.34}	-22.79 ^{+1.30} _{-0.83}	-0.86 ^{+0.34} _{-0.40}	25
5, Sc	19.03 ^{+0.83} _{-0.46}	3.40 ^{+1.08} _{-0.92}	-22.32 ^{+1.10} _{-0.49}	-19.98 ^{+1.34} _{-1.54}	-22.59 ^{+1.24} _{-0.52}	-1.06 ^{+0.62} _{-0.28}	30
6, Scd	19.70 ^{+0.74} _{-0.98}	2.93 ^{+0.71} _{-1.13}	-21.24 ^{+1.45} _{-0.42}	-17.38 ^{+0.56} _{-1.74}	-21.51 ^{+1.14} _{-0.69}	-1.34 ^{+0.22} _{-0.11}	7
7, Sd	21.05 ^{+0.24} _{-1.77}	3.66 ^{+1.72} _{-0.67}	-20.90 ^{+0.83} _{-1.17}	-18.50 ^{+0.87} _{-0.48}	-21.11 ^{+0.87} _{-1.27}	-1.35 ^{+0.51} _{-0.10}	9
8, Sdm	20.18 ^{+0.54} _{-0.29}	4.00 ^{+0.26} _{-1.51}	-20.92 ^{+0.95} _{-0.57}	-17.48 ^{+1.69} _{-0.89}	-21.10 ^{+0.94} _{-0.75}	-1.68 ^{+0.41} _{-0.16}	4
9, Sm	21.10 ^{+0.44} _{-0.08}	4.23 ^{+0.51} _{-1.97}	-20.36 ^{+1.51} _{-0.29}	-17.77 ^{+2.75} _{-0.54}	-20.70 ^{+1.11} _{-0.42}	-1.17 ^{+0.05} _{-0.65}	3
10, Irr	21.14 ^{+0.00} _{-0.00}	1.99 ^{+0.00} _{-0.00}	-18.94 ^{+0.00} _{-0.00}	-15.73 ^{+0.00} _{-0.00}	-19.16 ^{+0.00} _{-0.00}	-1.37 ^{+0.00} _{-0.00}	1
Morphological Class							
-3 $\leq T \leq$ 0	20.17 ^{+0.37} _{-0.37}	7.63 ^{+2.84} _{-2.84}	-22.56 ^{+0.60} _{-0.60}	-22.31 ^{+0.89} _{-0.89}	-22.84 ^{+0.65} _{-0.65}	-0.21 ^{+0.09} _{-0.09}	2
$T = 1-3$	19.11 ^{+0.97} _{-0.67}	3.91 ^{+3.42} _{-2.07}	-22.55 ^{+1.37} _{-0.78}	-21.78 ^{+1.88} _{-1.05}	-22.91 ^{+1.47} _{-0.77}	-0.39 ^{+0.43} _{-0.38}	33
$T = 6-9$	20.43 ^{+0.77} _{-0.77}	3.62 ^{+1.20} _{-1.50}	-20.79 ^{+1.01} _{-1.12}	-17.92 ^{+1.32} _{-1.04}	-21.11 ^{+1.03} _{-1.19}	-1.35 ^{+0.29} _{-0.46}	23

magnitude corrections from equation 4 to the observed bulge magnitudes. Table 5 shows these *B*-band bulge (and disc) magnitudes and the logarithm of the ratio of their luminosities. This latter quantity is plotted in Figure 6. The *B*-band flux ratios obtained from Simien & de Vaucouleurs (1986), which are still used by many research groups (e.g. Springel et al. 2001; Mathis et al. 2002; De Lucia et al. 2006) to build galaxies and assign galaxy types, are up to 0.5 dex larger. If the $R^{1/4}$ -derived flux ratios from Simien & Vaucouleurs were corrected for dust, then they would be greater still. While our galaxy parameters have been corrected for dust, they

have also been derived using $R^{1/n}$ rather than $R^{1/4}$ bulge models which, collectively, results in smaller flux ratios.

Having corrected the *B*-band *B/D* ratios for dust does not imply that they should be equal to the *K*-band values. In fact, differences are expected and will reflect the varying stellar populations of the bulges and discs. For example, a redder intrinsic (i.e. before the effects of dust) SED for a bulge will result in a larger *B/D* ratio in the *K*-band than in the *B*-band. In Figure 7 we have co-plotted the *K*- and *B*-band *B/D* values as a function of galaxy type. The S0–Sab galaxies have roughly the same *B/D* ratio, possibly

Table 7. *R* band parameters. The median, $\pm 68/2$ per cent of the distribution on either side of the median, is shown as a function of galaxy type (Column 1). Column 2: Bulge magnitude, obtained from the observed flux corrected using equation 4. Column 3: Disc magnitude, obtained from the observed flux corrected using equation 3. Column 4: Bulge-to-disc flux ratio using columns 2 and 3. Column 5: Number of data points.

Type	M_{bulge}	M_{disc}	$\log(B/D)$	#
1	2	3	4	5
Morphological Type				
-3, -2, -1, S0	0
0, S0/a	-22.45 ^{+1.35} _{-0.41}	-23.51 ^{+1.50} _{-0.03}	-0.34 ^{+0.10} _{-0.07}	3
1, Sa	-21.96 ^{+2.15} _{-0.45}	-21.96 ^{+0.88} _{-0.86}	-0.28 ^{+0.47} _{-0.08}	10
2, Sab	-21.28 ^{+1.83} _{-1.39}	-21.99 ^{+0.64} _{-1.43}	-0.33 ^{+0.45} _{-0.89}	9
3, Sb	-20.58 ^{+2.50} _{-1.32}	-22.65 ^{+1.36} _{-0.59}	-0.72 ^{+0.35} _{-0.34}	35
4, Sbc	-19.48 ^{+1.19} _{-1.89}	-22.27 ^{+1.19} _{-0.76}	-0.96 ^{+0.42} _{-0.44}	36
5, Sc	-19.33 ^{+1.13} _{-1.27}	-22.13 ^{+0.90} _{-0.53}	-1.07 ^{+0.45} _{-0.30}	47
6, Scd	-18.21 ^{+1.27} _{-0.98}	-21.48 ^{+1.47} _{-0.48}	-1.38 ^{+0.36} _{-0.12}	19
7, Sd	-17.22 ^{+1.22} _{-1.39}	-20.28 ^{+0.72} _{-1.63}	-1.38 ^{+0.47} _{-0.50}	18
8, Sdm	-16.75 ^{+0.83} _{-1.21}	-20.61 ^{+0.75} _{-0.44}	-1.46 ^{+0.21} _{-0.19}	7
9, Sm	-16.61 ^{+1.05} _{-0.59}	-19.50 ^{+0.60} _{-1.19}	-1.16 ^{+0.03} _{-0.27}	7
10, Irr	-16.77 ^{+0.68} _{-0.68}	-19.23 ^{+0.35} _{-0.35}	-0.99 ^{+0.13} _{-0.13}	2
-3 $\leq T \leq 0$	-22.45 ^{+1.35} _{-0.41}	-23.51 ^{+1.50} _{-0.03}	-0.34 ^{+0.10} _{-0.07}	3
$T = 1-3$	-21.04 ^{+1.94} _{-1.14}	-22.44 ^{+1.23} _{-0.86}	-0.60 ^{+0.44} _{-0.42}	54
$T = 6-9$	-17.44 ^{+1.50} _{-1.21}	-20.61 ^{+1.07} _{-1.28}	-1.36 ^{+0.32} _{-0.33}	51
Morphological Class				

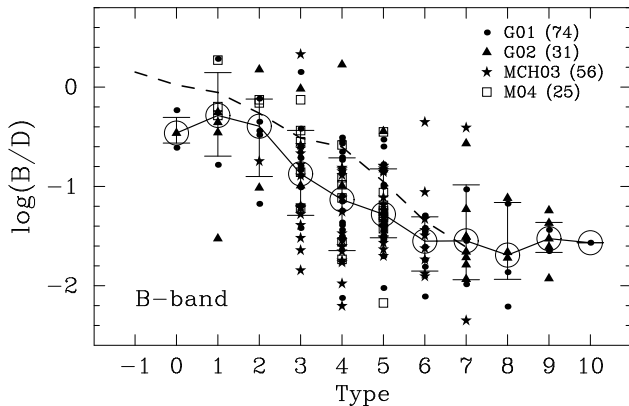


Figure 6. Logarithm of the *B*-band, bulge-to-disc flux ratio as a function of galaxy Type (see Table 5, column 7). The dashed line traces the *B*-band values from Simien & de Vaucouleurs (1986).

indicating similar stellar population, i.e. if the bulge is red, then the disc will also be red (Peletier & Balcells 1996). Although we do caution that other factors may be at play. Laurikainen et al. (2005) were careful to separate the bar flux from the bulge flux in their *K*-band analysis of early-type disc galaxies while Balcells et al.'s (2003) *K*-band sample did not possess bars. The optical studies might have overly large *B/D* ratios due to the assignment of bar flux to the bulge.

The later type spiral galaxies tend to have a *B*-band $\log(B/D)$ value which is nearly some ~ 0.3 dex smaller than the *K*-band value. That is, for the intermediate and late-type spiral galaxies, the *B*-band *B/D* ratio is a factor of 2 smaller than the *K*-band ratio. The obvious interpretation is that the later types have bluer — younger and/or more metal poor — discs relative to their bulges. Regarding the

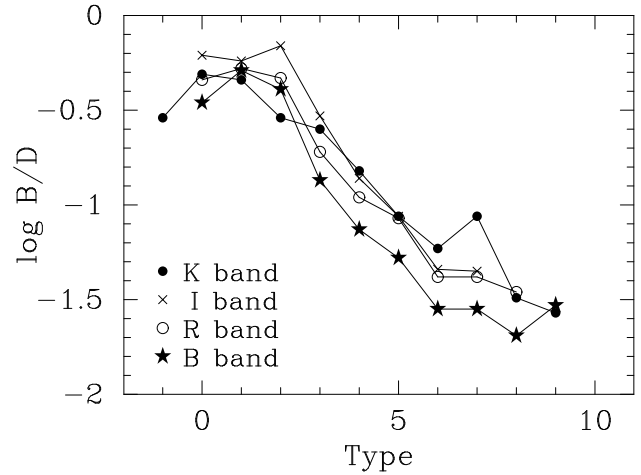


Figure 7. Median logarithm of the bulge-to-disc flux ratio as a function of galaxy Type. The number of galaxies involved in each data point can be seen in Tables 4 to 8.

Sm and irregular galaxies, the situation becomes somewhat mixed, and the diagram also suffers from low number statistics at this end. To provide a rough idea of the uncertainty on the plotted data points in Figure 7, we note that for a distribution with sample standard deviation equal to σ , the uncertainty on the mean is σ/\sqrt{N} , where N is the number of data points. From Table 4 we have $\sigma \sim 0.4$, while the value of N can be seen in Tables 4 to 8.

5 BIVARIATE DISTRIBUTIONS

Scaling relations, if found to exist, can (i) provide insight into the physical mechanisms which shape galaxies and (ii) supply helpful restrictions for simulations which try to match the real Universe and thereby understand it. In this section we present dust-corrected brightness-size distributions for galaxy discs (and also bulges and elliptical galaxies). Because the majority of disc galaxies consist of two main, physically distinct, components — a three-dimensional bulge and a relatively flat, two-dimensional disc — we do not treat the disc galaxies as single entities. Instead, we separately show bivariate distributions for the structural properties of the bulges and the discs.

The data from Dong & De Robertis (2006) is not included from here on. Their challengingly-shallow (eight second exposure) 2MASS images may be responsible for a number of apparent outliers which would slightly bias the fits in the following section if they had been included.

5.1 The μ_0 - $\log h$ distribution

Figure 8a shows the *K*-band distribution of face-on, central disc surface brightness μ_0 versus disc scalelength h . Both of these parameters have been fully corrected for the influence of dust. For exponential discs, one can easily transform this diagram so that it involves the effective radii, R_e , and effective surface brightnesses, μ_e . This is achieved by using $R_{e,\text{disc}} = 1.678h$ and $\mu_{e,\text{disc}} = \mu_0 + 1.822$, or the mean effective surface brightness within $R_{e,\text{disc}}$, which is such that $\langle \mu \rangle_{e,\text{disc}} = \mu_0 + 1.123$.

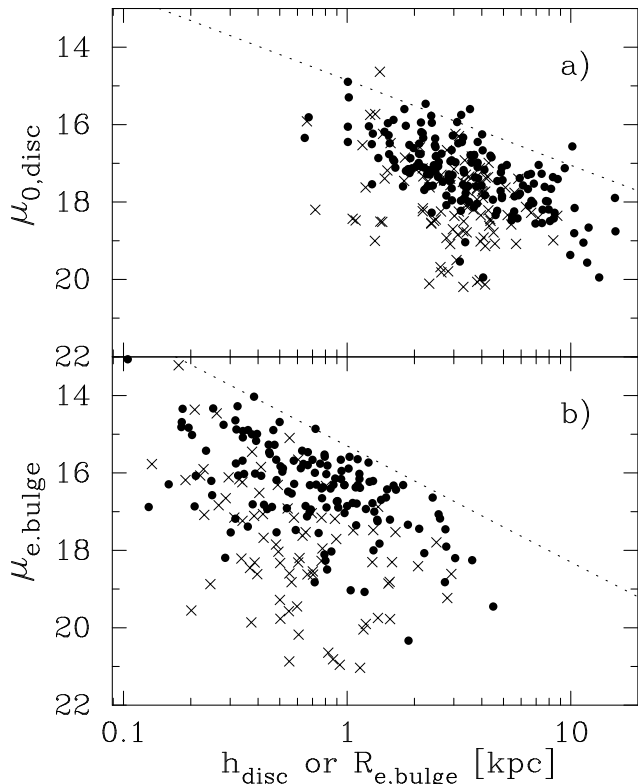


Figure 8. *K*-band. Top panel: Central disc surface brightness (corrected using equation 1) versus disc scalelength h (corrected using equation 2). Bottom panel: Bulge effective surface brightness (observed) versus the bulge effective radius R_e (observed). The upper bright envelope is traced here with the (empirical) lines $\mu_{0,\text{bright}} = 14.85 + 2.2 \log h$ (panel a) and $\mu_{e,\text{bright}} = 15.3 + 3.0 \log R_e$ (panel b). Galaxy types Sbc ($T = 4$) and earlier are denoted by the circles, while later galaxy types are denoted by the crosses.

Due to selection effects, small faint galaxies are likely to be missed and thus the lower-left of Figure 8a may be missing galaxies. The upper envelope in Figure 8a does however reflect a real cutoff in the distribution of galactic parameters, simply because bigger and brighter discs would be seen if they existed. The late-type disc galaxies can be seen to occupy a much broader region of this diagram than the early-type disc galaxies, and as such they are not particularly well represented by a linear surface brightness-size relation. Moreover, given the differing distribution of the early- and late-type disc galaxies (see also Figure 9), one can see that it is predominantly the late-type disc galaxies for which we may have an incomplete distribution in the lower-left quadrant.

Figure 9 shows the *B*-band μ_0 - $\log h$ relation in which the same general behaviour is observed. One of the immediate results that can be drawn from these figures is that the Freeman (1970) law, pertaining to a constant central disc surface brightness, requires modification. Not only do low surface brightness galaxies exist with fainter surface brightnesses — which has long been known (e.g. Disney 1976, 1998) — but the bright limit does not simply have the canonical Freeman surface brightness of 21.65 B-mag arcsec $^{-2}$. Instead, the bright limit is observed to depend strongly on

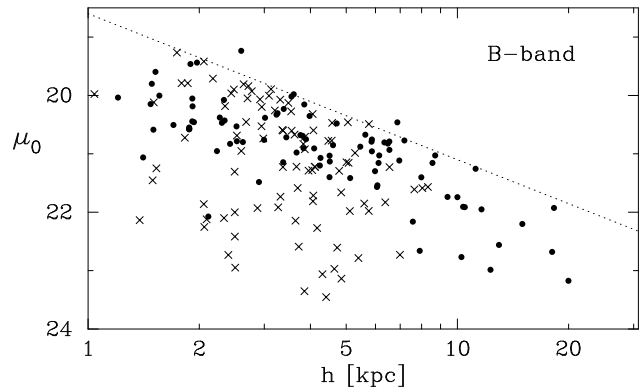


Figure 9. *B*-band. Central disc surface brightness (corrected using equation 1) versus disc scalelength (corrected using equation 2). Rather than a Freeman (1970) law of constant surface brightness, an upper bright envelope, which has been seen before (e.g. Graham 2001b and references therein), is evident. The empirically-fitted dotted line in this diagram is such that $\mu_{0,\text{bright}} = 18.6 + 2.5 \log h$. Galaxy types Sbc ($T = 4$) and earlier are denoted by circles, while later galaxy types are denoted by crosses. The noticeably broader distribution for the late-type disc galaxies has also been noted before (Graham & de Blok 2001).

disc size such that $\mu_{0,\text{bright}} \sim 2.5 \log h$ (Graham 2001b; Graham & de Blok 2001, and references therein). Obviously, this relation (quantified in section 5.3) also implies an improvement over the simple use of average disc scalelengths and central surface brightnesses to represent each of the (early-type) disc galaxy types.

5.2 The μ_e - $\log R_e$ distribution

The *K*-band distribution of bulge effective surface brightnesses μ_e and effective radii R_e are plotted in Figure 8b. As with the disc parameters, the bright envelope to this distribution is real and not an artifact of galaxy selection criteria. The bright boundary to the distribution is roughly described by the empirical relation $\mu_{e,\text{bright}} \sim 3 \log R_e$. Figure 8b qualitatively agrees with the (surface brightness)-size diagram in Binney & Merrifield (1998, their Fig.4.52) which was based on optical images of 66 galaxies from Kent (1985). The advances here are (i) sample size (ii) the influence of dust is less in the *K*-band and (iii) $R^{1/n}$ rather than $R^{1/4}$ models have been applied to every bulge.

5.3 The luminosity-size distribution

Given that $L = 2\pi I_0 h^2$ for exponential discs, the size-luminosity diagram is simply an alternative representation of the more traditionally used (surface brightness)-size diagrams seen in section 5.1. For convenience, both are shown here, although we emphasize that the upcoming size-luminosity relations could have been equally as well obtained by fitting lines to the data in Figures 8a and 9. The dashed lines in those figures have been mapped into Figure 10 which shows the (dust-corrected) disc magnitudes versus the (dust-corrected) disc scalelengths.

The early-type disc galaxy distribution in Figure 10 has been fit with a linear relation such that

$$\log h = a - \frac{b}{2.5}(M_{\text{disc}} + M_0), \quad (11)$$

and thus $h \propto L^b$. The quantity M_0 is simply a constant to help centralise the fit and thereby reduce the uncertainty on the intercept a . We have employed Feigelson & Babu's (1992) code SLOPES to perform six regression analyses: ordinary least squares of Y on X , $\text{OLS}(Y|X)$; and the inverse $\text{OLS}(X|Y)$; the line which bisects these two; minimisation of the perpendicular residuals (known as orthogonal regression); the geometric mean of $\text{OLS}(Y|X)$ and $\text{OLS}(X|Y)$, referred to as the reduced major axis regression line; and finally the arithmetic mean of the two OLS lines. Here, $Y = \log h$ and $X = M_{\text{disc}}$, and the results of the regression are shown in Tables 9 and 10. Table 10 also shows the results of the regressions for different galaxy types, although only in the K -band due to the numbers of galaxies involved.

From Graham & Driver (2005, their equation 12) one has that the absolute magnitude

$$M = \langle \mu \rangle_e - 2.5 \log[2\pi R_e^2] - 36.57, \quad (12)$$

with R_e in kpc. Therefore, for a disc with $n = 1$,

$$M_{\text{disc}} = (\mu_0 + 1.123) - 2.5 \log[2\pi(1.678h)^2] - 36.57. \quad (13)$$

From this relation one can readily express the disc size-luminosity relations (Tables 9 and 10) in terms of size and surface brightness. For example, combining equations 11 and 13 to eliminate M_{disc} , one has

$$\mu_0 = \frac{5b - 2.5}{b} \log h - M_0 + \frac{2.5a}{b} + 38.57. \quad (14)$$

If the typical central surface brightness $\mu_0 = -2.5 \log I_0$ was constant for the discs, although we know from Figures 8 and 9 that it is not, then one would find $h \sim L^{0.5}$. While a symmetrical regression of the optical data suggests $h \propto L^{0.75 \pm 0.04}$ for the discs of early-type disc galaxies (Table 9), the near-infrared data has a slope which is smaller, albeit only at the $\sim 1.5\sigma$ level.

A quick visual inspection of Figure 10 reveals that fitting to the full data set, i.e. both the early- and late-type disc galaxies, would produce $h \sim L^b$ relations with shallower slopes (smaller b values) than those reported in Table 9. We have not done this because (i) sample selection effects may have introduced an artificial boundary to the distribution of the late-type disc galaxies and (ii) from the $\mu_0 - \log h$ diagrams it was already clear that no real relation exists for the late-type disc galaxy population.

Before contrasting our results with others, we note that qualitative differences should not be surprising. We have derived intrinsic, fully dust corrected, *disc* scalelengths and luminosities from Sérsic $R^{1/n}$ bulge plus exponential disc decompositions. We first compare our K -band results with Courteau et al. (2007) who presented K -band *galaxy* luminosity-size relations for 360 2MASS galaxies binned into different galaxy types. At least for systems with small bulge-to-disc flux ratios, the distribution of disc light is roughly approximated by the distribution of the galaxy light. Indeed, as shown in Graham (2002, his Figure 6), galaxy half light radii are roughly equal to the half-light radii of the disc component.

Courteau et al. (2007) used an orthogonal regression analysis which can be seen in Tables 9 and 10 to give a shallower relation to our data than the three other symmet-

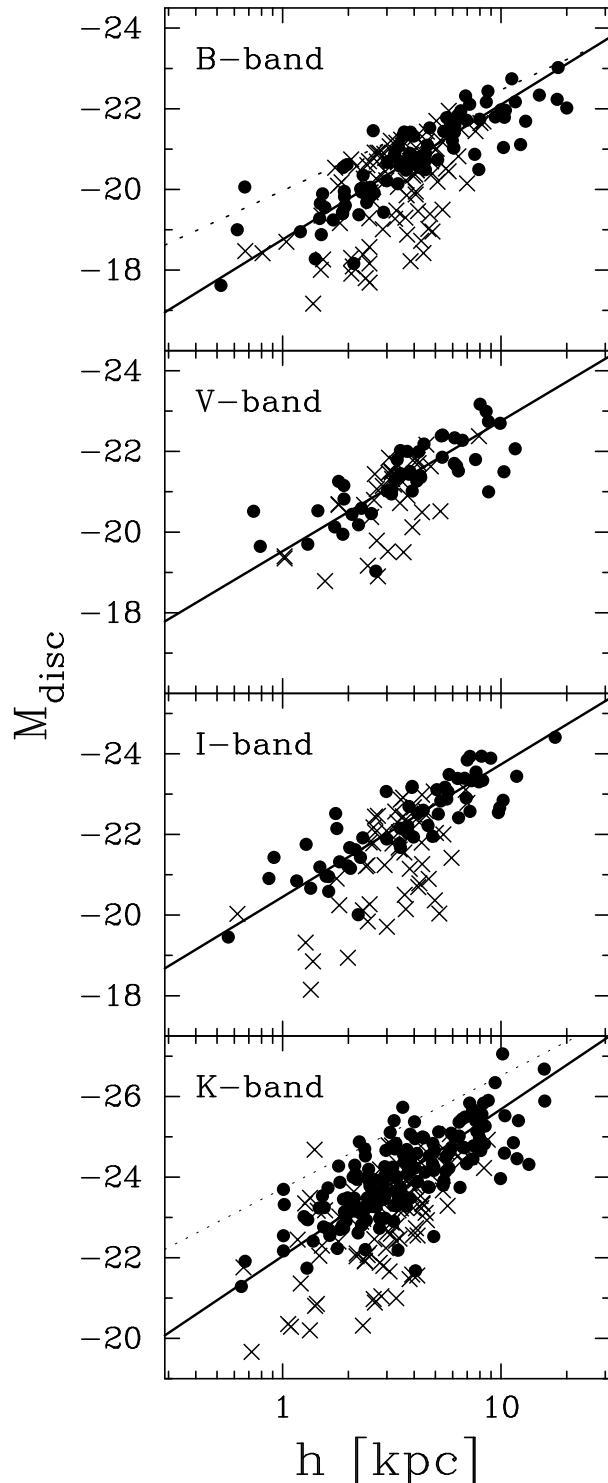


Figure 10. Inclination- and dust-corrected magnitude versus disc scalelength (via equation 2). Galaxy types Sbc ($T = 4$) and earlier are denoted by the circles, while later galaxy types are denoted by the crosses. The differing distributions between the galaxy types in these figures is directly related to their different distributions in the $\mu_0 - \log h$ plane (Figures 8 and 9). Similarly, evidence of a relation here is simply a re-representation of evidence for a relation in the $\mu_0 - \log h$ plane. The fitted lines to the discs of the early-type disc galaxies are given by the bisector regression of equation 11 (see Table 9). The dotted lines seen here denote the bright boundaries shown in Figures 8a and 9.

Table 9. Linear regression coefficients for the size-luminosity relations of disc galaxies with $T \leq 4$ (i.e., \leq Sbc). The fitted relation is such that $\log h = a - 0.4b(M_{\text{disc}} + M_0)$. The OLS bisector lines of regression are shown in Figure 10.

Method	B-band ($M_0 = 20$)		V-band ($M_0 = 21$)		I-band ($M_0 = 22$)		K-band ($M_0 = 24$)	
	a	b	a	b	a	b	a	b
OLS(Y X)	0.40 ± 0.02	0.65 ± 0.04	0.48 ± 0.03	0.59 ± 0.08	0.49 ± 0.02	0.65 ± 0.05	0.54 ± 0.01	0.49 ± 0.04
OLS(X Y)	0.34 ± 0.03	0.86 ± 0.06	0.42 ± 0.04	1.00 ± 0.14	0.46 ± 0.03	0.89 ± 0.07	0.54 ± 0.02	0.93 ± 0.07
OLS bisector	0.37 ± 0.02	0.75 ± 0.05	0.46 ± 0.03	0.77 ± 0.09	0.47 ± 0.02	0.76 ± 0.05	0.54 ± 0.02	0.69 ± 0.03
Orthogonal	0.38 ± 0.02	0.71 ± 0.05	0.47 ± 0.04	0.71 ± 0.11	0.48 ± 0.02	0.73 ± 0.06	0.54 ± 0.01	0.59 ± 0.04
Reduced major axis	0.37 ± 0.02	0.75 ± 0.05	0.46 ± 0.03	0.77 ± 0.09	0.47 ± 0.02	0.76 ± 0.05	0.54 ± 0.02	0.67 ± 0.04
Mean OLS	0.37 ± 0.02	0.75 ± 0.05	0.45 ± 0.03	0.79 ± 0.09	0.47 ± 0.02	0.77 ± 0.05	0.54 ± 0.02	0.71 ± 0.04

Table 10. Linear regression coefficients for the K-band disc size-luminosity relations of different disc galaxy types: $\log h = a - 0.4b(M_{\text{disc}} + 24)$.

Method	$T = 1 \pm 1$ (Sa)		$T = 3 \pm 1$ (Sb)		$T = 5 \pm 1$ (Sc)		$T \geq 6$ (\geq Scd)	
	a	b	a	b	a	b	a	b
OLS(Y X)	0.51 ± 0.03	0.53 ± 0.06	0.55 ± 0.02	0.48 ± 0.04	0.58 ± 0.02	0.34 ± 0.03	0.61 ± 0.03	0.21 ± 0.05
OLS(X Y)	0.51 ± 0.04	1.15 ± 0.17	0.54 ± 0.02	0.92 ± 0.07	0.64 ± 0.02	0.73 ± 0.07	0.87 ± 0.08	0.63 ± 0.12
OLS bisector	0.51 ± 0.03	0.80 ± 0.07	0.54 ± 0.02	0.68 ± 0.04	0.61 ± 0.01	0.52 ± 0.03	0.73 ± 0.03	0.40 ± 0.04
Orthogonal	0.51 ± 0.03	0.70 ± 0.09	0.55 ± 0.02	0.58 ± 0.05	0.58 ± 0.02	0.39 ± 0.04	0.62 ± 0.03	0.23 ± 0.05
Reduced major axis	0.51 ± 0.03	0.78 ± 0.08	0.54 ± 0.02	0.67 ± 0.04	0.60 ± 0.01	0.50 ± 0.03	0.70 ± 0.03	0.36 ± 0.03
Mean OLS	0.61 ± 0.03	0.84 ± 0.09	0.54 ± 0.02	0.70 ± 0.04	0.61 ± 0.01	0.53 ± 0.04	0.74 ± 0.04	0.42 ± 0.05

rical regression analyses which we used. For our (potentially sample-selection biased) late-type galaxies ($T > 5$) we have the K-band relation $h \sim L^{0.23 \pm 0.05}$ (orthogonal regression), which is in fair agreement with Courteau et al.’s relation $L_{\text{gal}}^{0.31 \pm 0.17}$ for Sd galaxies (their Table 3). For our Sc, Sb and Sa galaxy samples we find exponents of 0.39 ± 0.04 , 0.58 ± 0.05 and 0.70 ± 0.09 respectively. Such an increase is in qualitative agreement with Courteau et al. who report values of 0.39 ± 0.03 , 0.43 ± 0.04 and 0.57 ± 0.04 .

Courteau et al. additionally presented a size-luminosity diagram for 1300 disc galaxies with I-band imaging, reporting $h \sim L^{0.33 \pm 0.02}$ (Sc galaxies), $h \sim L^{0.37 \pm 0.02}$ (Sb galaxies) and $h \sim L^{0.55 \pm 0.05}$ (Sa galaxies). When we fit all of our I-band data, i.e. late- and early-type disc galaxies, we obtain $h \sim L^{0.45 \pm 0.05}$ (orthogonal regression), while our fit to the S0-Sbc galaxies is notably steeper, with $h \sim L^{0.73 \pm 0.06}$ (orthogonal regression). Due to our smaller number of galaxies with I-band data, we do not attempt a finer division of galaxy type.

We have also compared our result with the disc galaxy size-luminosity relations in Shen et al. (2003). In their work they show the r' galaxy luminosity versus the galaxy half light radius. At the luminous end of Shen et al.’s size-luminosity diagram ($M_{r'} < -20$ mag), they report that radius varies with $L^{0.53}$. They performed an OLS(Y|X) regression analysis on binned data, making it additionally difficult to perform an exact comparison with our results. At magnitudes brighter than $M_{r'} = -20$ mag, their Figure 5 reveals that the early-type disc galaxies follow the relation $h \sim L^{0.58}$. At lower-luminosities they report shallower slopes.

Shen et al. (2003) assumed that galaxies with concentration parameters less than 2.86 are disc galaxies. When dealing with bright galaxy samples this is a reasonable approximation which has been illustrated with visually classified samples. However, a problem occurs when one expands one’s sample to fainter magnitudes because most dwarf elliptical galaxies have $n < 2$ and thus concentrations less than ~ 2.86 (Graham et al. 2005, their table 1). As a re-

sult, faintward of ~ -19 r' -mag (~ -20 z' -mag) in Shen et al.’s Figures 4-7 (and 10), one does not know if the systems are actually early- or late-type galaxies. This can however be resolved by looking at Shen et al.’s Figures 8-9, in which it becomes apparent that the curved nature of their disc galaxy size-luminosity relation is due to the mixing of galaxy types at the low-luminosity end. This implies that (i) the curved size-luminosity relations for late-type galaxies in Table 1 from Shen et al. are not appropriate and (ii), the linear size-luminosity relations for early-type galaxies in their Table 1 are also not appropriate at faint magnitudes. This has prompted us to revisit the size-luminosity diagram for elliptical galaxies, to which we are able to add and compare the distribution of bulges.

5.3.1 Elliptical galaxies

From $-18 < M_B < -13$ mag, the effective radii of dwarf elliptical galaxies display no real trend with magnitude but instead scatter around a value of ~ 1 kpc (Smith Castelli et al. 2008; Dabringhausen et al. 2008; Figure 11a). This often over-looked result was previously shown in Binggeli & Jerjen (1998) and actually also noted in Shen et al. (2003, their Figures 8 and 9) but the implications of which were not propagated into all of their diagrams.

The curved distribution of data points in Figure 11a can be predicted (see the line in this figure) from the following linear $M - \mu_0$ and $M - \log n$ (Figure 11b) relations for elliptical galaxies. Using equations 7, 9 and 12 from Graham & Driver (2005), one has an expression involving M , R_e , μ_0 and n for any Sérsic profile. For elliptical galaxies, the μ_0 term in this (not shown) expression can be replaced with M via the empirical relation

$$M_B = \frac{2}{3}\mu_{0,B} - 29.5 \quad (15)$$

from Graham & Guzmán (2003), to give the relation

$$\log R_e[\text{kpc}] = 1.137 + 0.217b_n + \frac{M_B}{10} + 0.5 \log \left[\frac{b_n^{2n}}{n\Gamma(2n)e^{bn}} \right], \quad (16)$$

where $b_n \approx 1.9992n - 0.3271$, for $0.5 < n < 10$ (Capaccioli 1989). The value of n can also be expressed in terms of M_B using the empirical relation

$$n = 10^{-(14.3+M_B)/9.4} \quad (17)$$

from Graham & Guzmán (2003). This is how the line in Figure 11a was derived. It can be seen to match the behaviour of the data rather well, which has (only) an approximately linear behaviour ($R_e \propto L^{0.9}$ from the data in Figure 11a) at luminosities brighter than $M_B \sim -19$ mag. The gradual curvature in the bright end of this $L - R$ relation is independently supported by the data in Liu et al. (2008, their Fig.12), for which their brightest cluster galaxies (when using 25 r -mag/arcsec² isophotal magnitudes) have $R_{50} \propto L^{0.88}$. The exponential-like envelopes of cD galaxies (Seigar et al. 2007) does however complicate the derivation of reliable brightest cluster galaxy parameters and we do not explore this issue here.

The curved size-luminosity relation for elliptical galaxies, predicted from two linear relations, is probably not a fundamental relation. Due to the continually varying slope of the $L - R$ relation, the mean slope for dwarf and bright elliptical galaxies will be different. This is, however, not evidence for two disjoint species of galaxies. Similarly, as explained in Graham & Guzmán (2003), the continually curved size-(effective surface brightness) relation for elliptical galaxies is not evidence for two distinct types of galaxy. Instead, the curved relation is expected from the linear relations which dwarf and luminous elliptical galaxies are observed to co-define.

Having derived the curved size-luminosity relation for elliptical galaxies from two linear relations, we examine why the bright end slope is different to that reported by Shen et al. (2003). Shen et al. used Petrosian quantities for the luminous elliptical galaxies, however Petrosian magnitudes miss the outer flux in galaxies, and increasingly so for brighter galaxies. While the Petrosian magnitude is therefore fainter than the total magnitude, it is actually the Petrosian half flux radii R_{50} which is most heavily impacted in comparison with the effective half light radii R_e . This is quantified in Graham et al. (2005). Looking at Shen et al.'s Figure 4, one can see that their early-type galaxies display a linear size-luminosity relation from $-19.75 > M_{r'} > -23.75$. From Fukugita et al. (1995) we have $B - r' = 1.32$ and so the above magnitude range corresponds to $-18.43 > M_B > -22.43$. From Figure 11b we see that this magnitude range corresponds to a range in Sérsic index from 3 to 7. We can now use the relation $R_{50} \approx [1 - 6.0 \times 10^{-6} (R_{90}/R_{50})^{8.92}] R_e$ from Graham et al. (2005) to quantify the difference between the Petrosian half light radii R_{50} (used by Shen et al.) and the effective half light radii R_e (used in Figure 11a). When $n = 7$ ($R_{90}/R_{50} = 3.62$), $R_{50} = 0.42R_e$. When $n = 3$ ($R_{90}/R_{50} = 3.17$), $R_{50} = 0.82R_e$. Such a systematic reduction to the radii, as the elliptical galaxy luminosity increases, results in a reduction (of a factor $\log[4.2/0.82] \approx 0.71$) to the exponent b in the relation $R \propto L^b$, and likely explains why Shen et al. (2003) find $R_{50} \propto L_{\text{Petrosian}}^{0.60}$. The Sérsic radii from Blanton et al. (2005) — which Shen et al. additionally used — are also known to systematically underestimate the true effective half light radii as the Sérsic index increases (see Figure 9 from Blanton et al. 2005). Underestimation also occurs when using $R^{1/4}$ models to describe systems with $n > 4$

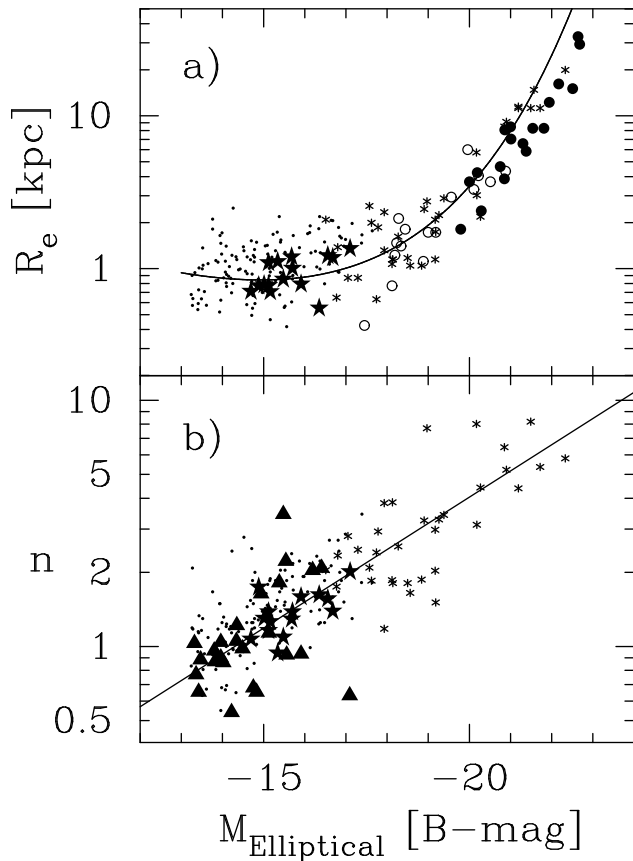


Figure 11. B -band. Panel a) Luminosity-size diagram for elliptical galaxies. The data have come from the compilation in Graham & Guzmán (2003, see their Figure 9). The line is not a fit to the data, but a prediction based upon the linear relations between absolute magnitude and central surface brightness (Graham & Guzmán 2003, their Figure 9f) and absolute magnitude and the logarithm of the Sérsic index — shown here in panel b) for convenience but taken from Graham & Guzmán (2003, their Figure 10). A fixed change in Sérsic index n , for example $\delta n = 1$, causes a large change to the profile when n is small, but only a small change when n is large. Because of this, plots of galaxy parameters such as magnitude or colour will appear curved (flattening at large n) rather than linear, if they are plotted against n rather than $\log n$.

(see Trujillo et al. 2001, their Figure 4) which may explain why Bernardi et al. (2003) report that $R \sim L^{0.63}$. Therefore, while the above results are not necessarily wrong, it does highlight that if we are to compare theory (e.g. Mayer, Governato & Kaufmann 2008) and observations, it is important that we measure radii and luminosities in a physically appropriate and consistent manner.

5.3.2 Bulges

Finally, with new data in hand, the K -band size-luminosity distribution for the bulges is shown in Figure 12. No real trend is evident and we refrain from fitting a relation to this scatter diagram. We can however explore if the upper boundary in this Figure is real. Potentially, just as low surface brightness disc galaxies avoided detection due to effectively being hidden by the sky background flux (Disney

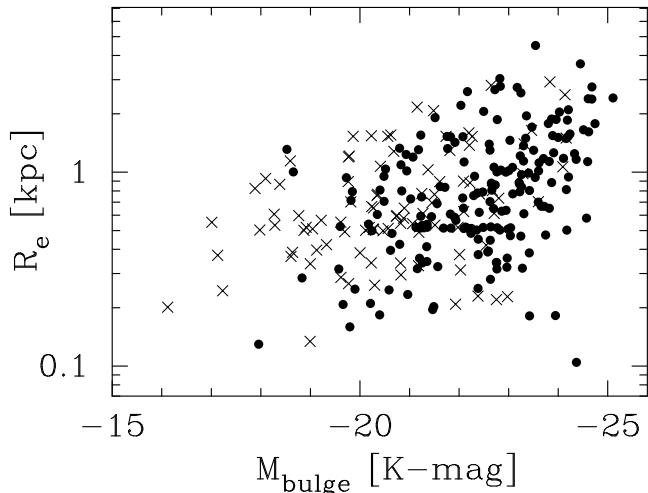


Figure 12. *K*-band. Size-luminosity diagram for bulges. Galaxy types Sbc ($T = 4$) and earlier are denoted by the circles, while later galaxy types are denoted by the crosses.

1976; Longmore et al. 1982; Davies et al. 1988), a population of large, low surface brightness bulges (which could populate the upper left portion of Figure 12) may be submerged beneath the flux of their associated discs. The existence of such bulges is likely to be rare for the simple fact that galaxies in which no bulge is detected, i.e. bulgeless galaxies, are rare. If a bulge was to exist with, for example, $R_e = 3$ kpc and an absolute *K*-band magnitude of -20 mag, then it would have a mean effective surface brightness of 20.95 *K*-mag arcsec $^{-2}$ (Graham & Driver 2005, their eq.12). If this bulge had a Sérsic index $n = 1$, then it would have a *K*-band central surface brightness of 19.83 mag arcsec $^{-2}$. If bright enough relative to the host disc, this will result in a central protrusion of the galaxy light profile, above that of the disc profile. For late-type, bulgeless disc galaxies (say Sd or later), we can see from Table 3 that their central disc surface brightnesses are not bright enough to hide such a bulge. On the other hand, a bulge with $R_e = 3$ kpc and an absolute *K*-band magnitude of -18 mag, and thus a central surface brightness of 21.83 mag arcsec $^{-2}$, could be hidden. Although we note that if the ratio $\langle R_e/h \rangle \approx 0.2 - 0.25$ holds, it would require the late-type disc galaxy has a scalelength around 12-15 kpc, something which is not seen in Figures 8 or 9. We therefore tentatively conclude that the upper boundary in Figure 12 is real.

In Figure 13 we have very crudely adjusted the *K*-band bulge magnitude to the *B*-band by using $B - K = 4$, so as to place the bulges in the same diagram as elliptical galaxies. While they roughly overlap with the dwarf elliptical galaxies, at a given magnitude they scatter to smaller sizes. This is somewhat reminiscent of their behaviour in the magnitude - Sérsic index diagram, where, for a given magnitude, the bulges scatter to smaller Sérsic indices than the dwarf elliptical galaxies do (Graham 2001a, his Fig.14).

6 SUMMARY

Most bright galaxies in the Universe today are spiral galaxies. Loveday (1996) has estimated that two-thirds of galaxies

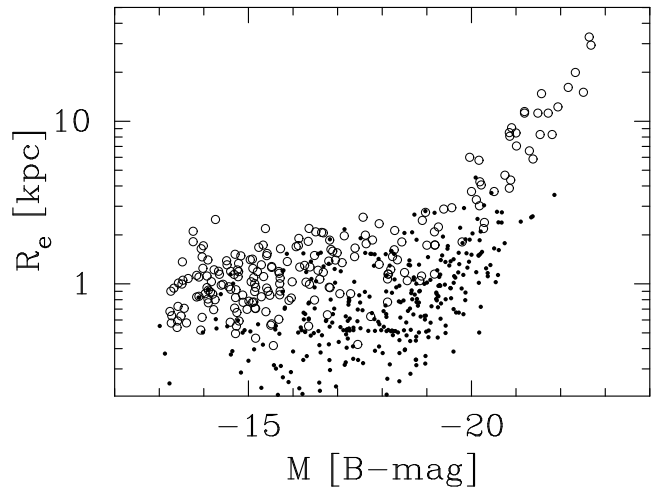


Figure 13. Size-luminosity diagram for elliptical galaxies (open circles) and bulges (dots). The *K*-band bulge magnitudes have been shifted to the *B*-band using a constant $B - K$ colour of 4.0.

brighter than $M_V = -18$ mag are spiral galaxies and Lintott et al. (2008) report that the elliptical to spiral ratio is 0.57 for galaxies with $M_r < -19$ mag; the actual number of disc (i.e. spiral plus lenticular) galaxies is greater still. Discs are well known to contain dust which biases our measurements of their physical parameters and also that of their embedded bulges. Matching observational data from over 10,000 galaxies (Allen et al. 2006) with radiative transfer measurements from sophisticated, three-dimensional models of disc galaxies with dust (Popescu et al. 2000; Tuffs et al. 2004), Driver et al. (2007) has recently provided a highly useful calibration of these models. From this, equations to correct the observed scalelength and surface brightness for inclination and dust are derived and presented here (equations 1 and 2). In the optical bands, dust can bias the measured disc scalelength and surface brightness by 40 per cent and ~ 0.5 mag arcsec $^{-2}$, respectively, while the disc magnitude can be in error by up to 1 magnitude. Corrections for dust are therefore quite significant. We remark that programs to measure the evolution of disc galaxy parameters may need to additionally consider the evolution of their dust.

These attenuation-inclination corrections enabled us to provide a modern, quantitative measure of the intrinsic physical properties of disc galaxies in the local ($z < 0.03 - 0.04$) Universe. We have done this by converting the observed properties of disc galaxies into their intrinsic (not simply face-on) dust free values. This is desirable because comparison between theory and observations, which is used to facilitate our understanding of galaxy formation and evolution, is hampered when one's observational measurements are compromised by the attenuating effects of dust.

Using a sample of galaxies which have been carefully fitted with Sérsic $R^{1/n}$ bulges plus exponential discs, this paper presents intrinsic structural properties for disc galaxies as a function of galaxy type. This work improves upon measurements obtained using $R^{1/4}$ models for every bulge, and provides inclination- and dust-corrected disc scalelengths, central surface brightnesses and magnitudes in optical and near-infrared passbands.

In addition, we present inclination- and dust-corrected

bulge-to-disc flux ratios in several passbands, and K -band bulge-to-disc size ratios, as a function of morphological type. For a given galaxy type, the logarithm of the B -band bulge-to-disc flux ratios from Simien & de Vaucouleurs (1986) are as much as ~ 0.5 dex larger than the values obtained here. This is predominantly due to the best-fitting Sérsic $R^{1/n}$ bulge models having $n < 4$, while Simien & de Vaucouleurs force fit an $R^{1/4}$ model to every bulge. In general, the median dust-corrected bulge-to-total flux (mass) ratios are less than $1/3$ ($1/2$), which may provide a useful new restraint on some simulations which tend to produce larger ratios. Given the observed range of bulge Sérsic indices from ~ 0.5 to ~ 4 , we advocate the use of Prugniel & Simien's (1997) density model which was developed to match deprojected Sérsic profiles, rather than only matching a deprojected $R^{1/4}$ profile.

Rather than only dividing the galaxies into early- and late-type bins based upon their colour and/or concentration index, catalogued Hubble types were available for all of our galaxies. This has also enabled us to perform our analysis on a sample of disc galaxies, rather than an unknown blend of early- and late-type galaxies which have similar concentration indices at low magnitudes. However no attempt has been made to measure volume densities given the ad-hoc galaxy selection criteria. Although we note that in Driver et al. (2007, 2008), which contains expressions to correct bulge and disc magnitudes in a range of optical and near-infrared passbands, including the Sloan Digital Sky Survey (SDSS; York et al. 2000) filter set, we have already done this for the luminosity density of bulges and discs.

We have presented updated (surface brightness)-size diagrams for bulges and discs and investigated the size-luminosity relations. We reveal that the discs of late-type disc galaxies occupy a broad region in these diagrams and are not well represented by linear relations. In contrast, the discs of early-type disc galaxies appear to reside over a narrower territory, defining the bright envelope to these distributions. We have additionally presented the size-luminosity relation for bulges and elliptical galaxies, emphasizing that a linear relation is inappropriate. The bulges of disc galaxies are shown to overlap with, but additionally scatter to smaller sizes than, the distribution of similarly luminous elliptical galaxies.

To conclude, while the amount of dust in galaxy discs is roughly one thousand times less than the stellar mass, it can have a large influence on the observed properties of galaxies. In this study we have corrected for the influence of dust in order to obtain the intrinsic stellar properties of galaxies. Such characteristic physical properties, and indeed their bivariate distributions and possible scaling relations, are not only interesting in their own right but provide valuable $z = 0$ constraints for models of galaxy evolution.

7 ACKNOWLEDGMENTS

We thank Cristina Popescu and Richard Tuffs for kindly proof-reading this manuscript and providing helpful feedback. We also thank Ileana Vass for kindly faxing us select pages from the RC3. We are grateful to both the Australian National University summer school program which initiated this project in late 2005, and to the Swinburne University of Technology's Researcher Development Scheme which

enabled completion of this project in 2007. This research has made use of the NASA/IPAC Extragalactic Database (NED),

REFERENCES

- Abadi, M.G., Navarro, J.F., Steinmetz, M., Eke, V.R. 2003a, ApJ, 591, 499
- Abadi, M.G., Navarro, J.F., Steinmetz, M., Eke, V.R. 2003b, ApJ, 597, 21
- Allen, P. D., Driver, S. P., Graham, A. W., Cameron, E., Liske, J., & de Propris, R. 2006, MNRAS, 371, 2
- Almeida, C., Baugh, C. M., Wake, D. A., Lacey, C. G., Benson, A. J., Bower, R. G., & Pimbblet, K. 2008, MNRAS, 466
- Andersen, D. R., Bershad, M. A., Sparke, L. S., Gallagher, J. S., III, & Wilcots, E. M. 2001, ApJ, 551, L131
- Andredakis, Y.C., Peletier, R.F., & Balcells, M. 1995, MNRAS, 275, 874
- Andredakis, Y.C., Sanders, R.H., 1994, MNRAS, 267, 283
- Aragón-Salamanca, A., Bedregal, A. G., & Merrifield, M. R. 2006, A&A, 458, 101
- Athanassoula, E. 2008, IAU Symposium 245 "Galactic bulges", M. Bureau et al. eds (arXiv:0802.0151)
- Bailin, J., Harris, W.E. 2008, ApJ, in press (arXiv:0803.1274)
- Balcells, M., Graham, A. W., Domínguez-Palmero, L., & Peletier, R. F. 2003, ApJ, 582, L79
- Balcells, M., Graham, A. W., & Peletier, R. F., 2007, ApJ, in press (astro-ph/0404381)
- Barnes, E.I., & Sellwood, J.A. 2003, AJ, 125, 1164
- Barway, S., Kembhavi, A., Wadadekar, Y., Ravikumar, C.D., Mayya, Y.D., 2007, ApJL, 661, L37
- Bekki, K., Couch, J., & Yasuhiro, S. 2002, ApJ, 577, 651
- Bernardi, M., et al. 2003, AJ, 125, 1849
- Binggeli, B., Jerjen, H. 1998, A&A, 333, 17
- Binney, J., & Merrifield, M. 1998, Galactic astronomy / James Binney and Michael Merrifield. Princeton, NJ : Princeton University Press, 1998. (Princeton series in astrophysics)
- Blakeslee, J.P., et al., 2002, MNRAS, 330, 443
- Blanton, M. R., et al. 2005, AJ, 129, 2562
- Boissier S., Boselli A., Buat V., Donas J., Milliard B., 2004, A&A, 424, 465
- Boroson, T. 1981, ApJS, 46, 177
- Bower, R.G., Benson, A.J., Malbon, R., Helly, J.C., Frenk, C.S., Baugh, C.M., Cole, S., & Lacey, C.G. 2006, MNRAS, 370, 645
- Bournaud, F., Combes, F., Jog, C.J., & Puerari, I. 2005, A&A, 438, 507
- Brown, R.J.N., et al. 2003, MNRAS, 341, 747
- Bruzual, G., & Charlot, S. 2003, MNRAS, 344, 1000
- Calura, F., Pipino, A., Matteucci, F. 2008, in XIXemes Rencontres de Blois (arXiv:0801.2551)
- Caon, N., Capaccioli, M., & D'Onofrio, M. 1993, MNRAS, 265, 1013
- Capaccioli, M. 1989, in The World of Galaxies, ed. H.G. Corwin, L. Bottinelli (Berlin: Springer-Verlag), 208
- Cardelli, J. A., Clayton, G. C., & Mathis, J. S. 1989, ApJ, 345, 245
- Carollo, C. M., Scarlata, C., Stiavelli, M., Wyse, R. F. G., & Mayer, L. 2007, ApJ, 658, 960
- Castro-Rodríguez, N. & Garzón, F. 2003, A&A, 411, 55
- Ciotti, L., Pellegrini, S., Renzini, A., & D'Ercole, A. 1991, ApJ, 376, 380
- Cole, S., Lacey, C.G., Baugh, C.M., Frenk, C.S. 2000, MNRAS, 319, 168
- Courteau, S., Dutton, A. A., van den Bosch, F. C., MacArthur, L. A., Dekel, A., McIntosh, D. H., & Dale, D. A. 2007, ApJ, 671, 203

- Courteau, S., de Jong, R. S., & Broeils, A. H. 1996, *ApJ*, 457, L73
- Cox D.P., 2000, *Allen's Astrophysical quantities*, New York: AIP Press; Springer, p.341
- Croft, R.A.C., Di Matteo, T., Springel, V., Hernquist, L. 2008, *MNRAS*, submitted (arXiv:0803.4003)
- Croton, D.J., et al. 2006, *MNRAS*, 365, 11
- Dabringhausen, J., Hilker, M., & Kroupa, P. 2008, *MNRAS*, in press (arXiv:0802.0703)
- Davies, J.I., Phillipps, S., & Disney, M.J. 1988, *MNRAS*, 231, 69p
- de Jong, R.S. 1996b, *A&A*, 313, 45
- de Jong, R.S. 1996a, *A&AS*, 118, 557
- de Jong, R.S., & van der Kruit, P.C., 1994, *A&AS*, 106, 451
- de Lucia, G., Springel, V., White, S.D.M., Croton, D., Kauffmann, G. 2006, *MNRAS*, 366,499
- de Vaucouleurs, G., 1948, de Vaucouleurs, G., 1948, *Annales d'Astrophysique*, 11, 247
- de Vaucouleurs, G., 1957, *AJ*, 62, 69
- de Vaucouleurs, G., 1958, *ApJ*, 128, 465
- de Vaucouleurs, G., de Vaucouleurs, A., Corwin, H.G., Jr., Buta, R.J., Paturel, G., & Fouque, P. 1991, Volume 1-3, XII, 2069 p.7, Springer-Verlag Berlin Heidelberg New York
- de Vaucouleurs, G., & Pence, W.D., 1978, *AJ*, 83, 1163
- Disney, M.J. 1976, *Nature*, 263, 573
- Disney, M.J. 1998, *IAU Colloquium 171*, ASP Conf. Ser.,J.I. Davies, C. Impey, and S. Phillipps, eds., 170, 11
- Dong, X.Y., & De Robertis, M.M. 2006, *AJ*, 131, 1236
- D'Onghia, E., Burkert, A., Murante, G., & Khochfar, S. 2006, *MNRAS*, 372, 1525
- D'Onofrio, M. 2001, *MNRAS*, 326, 1517
- Driver, S.P., Popescu, C.C., Tuffs, R.J., Liske, J., Graham, A.W., Allen, P.D., De Propriis, R., 2007, *MNRAS*, in press (arXiv:0704.2140)
- Driver, S.P., Popescu, C.C., Tuffs, R.J., Graham, A.W., Liske, J., Baldry, I.K., 2008, *ApJL*, in press (arXiv:0803.4164)
- Ebnetter, K., & Balick, B. 1985, *AJ*, 90, 183
- Ebnetter, K., Davis, M., & Djorgovski, S. 1988, *AJ*, 95, 422
- Einasto, J. 1965, *Trudy Inst. Astrofiz. Alma-Ata*, 5, 87
- Erwin, P., Vega Beltran, J.C., Graham, A.W., Beckman, J.E., 2003, *ApJ*, 597, 929
- Eskridge, P.B., et al. *ApJS*, 143, 73
- Feigelson, E.D., & Babu, G.J. 1992, *ApJ*, 397, 55
- Ferrarese, L., & Ford, H. 2005, *Space Science Reviews*, 116, 523
- Ferrari, F., Pastoriza, M.G., Macchetto, F., & Caon, N. 1999, *A&AS*, 136, 269
- Fitzpatrick, E.L. 1999, *PASP*, 111, 63
- Foyle, K., Courteau, S., Thacker, R. 2008, *MNRAS*, in press (arXiv:0803.2716)
- Freeman, K.C., 1970, *ApJ*, 160, 811
- Gadotti, D.A. 2008, *MNRAS*, 384, 420
- Giovanelli, R., Haynes, M.P., Salzer, J.J., Wegner, G., da Costa, L.N., & Freudling, W. 1995, *AJ*, 110, 1059
- Governato, F., et al. 2004, *ApJ*, 607, 688
- Governato, F., Willman, B., Mayer, L., Brooks, A., Stinson, G., Valenzuela, O., Wadsley, J., & Quinn, T. 2007, *MNRAS*, 374, 1479
- Graham, A.W. 2001a, *AJ*, 121, 820 (Addendum, 2003, *AJ*, 125, 3398)
- Graham, A.W. 2001b, *MNRAS*, 326, 543
- Graham, A.W. 2002, *MNRAS*, 334, 721
- Graham, A.W. 2003, *AJ*, 125, 3398
- Graham, A.W. 2007, *MNRAS*, 379, 711
- Graham, A.W., & de Blok, W.J.G. 2001, *ApJ*, 556, 177
- Graham, A.W., & Driver, S.P. 2005, *PASA*, 22(2), 118 (astro-ph/0503176)
- Graham, A.W., & Driver, S.P. 2007, *MNRAS*, 380, L15
- Graham, A.W., Driver, S.P., Petrosian, V., Conselice, C.J., Bershad, M.A., Crawford, S.M., & Goto, T. 2005, *AJ*, 130, 1535
- Graham, A.W., & Guzmán, 2003, *AJ*, 126, 1787
- Graham, A.W., Merritt, D., Moore, B., Diemand, J., & Terzić, B. 2006a, *AJ*, 132, 2701
- Graham, A.W., Merritt, D., Moore, B., Diemand, J., & Terzić, B. 2006b, *AJ*, 132, 2711
- Graham, A.W., & Prieto, M., 1999, *ApJ*, 524, L23
- Grosbøl, P., Patsis, P.A., & Pompei, E. 2004, *A&A*, 423, 849
- Guthrie, B.N.G. *A&AS*, 1992, 93, 255
- Haynes, M.P., & Giovanelli, R. 1984, *AJ*, 89, 758
- Hernandez, X., & Cervantes-Sodi, B. 2006, *MNRAS*, 368, 351
- Hernandez-Toledo, H., Zendejas-Dominguez, J., & Avila-Reese, V. 2007, *AJ*, in press (arXiv:0705.2041)
- Hernquist, L. 1990, *ApJ*, 356, 359
- Holmberg, E. 1946, *Medd. Lund. Astron. Obs. Ser. II. No. 117*
- Hubble, E. 1926, *ApJ*, 64, 321
- Iodice, E., D'Onofrio, M., Capaccioli, M. 1997, *ASP Conf. Ser.*, 116, 841
- Iodice, E., D'Onofrio, M., Capaccioli, M. 1999, *ASP Conf. Ser.*, 176, 402
- Jerjen, H., Binggeli, B., & Freeman, K.C. 2000, *AJ*, 119, 593
- Kassin, S.A., de Jong, R.S., Pogge, R.W. 2006, *ApJS*, 162, 80
- Kodaira, K., Watanabe, M., & Okamura, S. 1986, *ApJS*, 62, 703
- Kormendy, J., & Kennicutt, R.C., Jr. 2004, *ARA&A*, 42, 603
- Kormendy, J. 2008, in *Formation and Evolution of Galaxy Bulges*, Proceedings IAU Symposium No. 245, 2007, M. Bureau et al. eds., in press (arXiv:0708.2104)
- Kornreich, D.A., Haynes, M.P., & Lovelace, R.V.E. 1998, *AJ*, 116, 2154
- Kent, S., 1985, *ApJS*, 59, 115
- Kent, S.M., Dame, T., & Fazio, G., 1991, *ApJ*, 378, 131
- Khosroshahi, H.G., Wadadekar, Y., & Kembhavi, A. 2000, *ApJ*, 533, 162
- Knapen, J.H., de Jong, R.S., Stedman, S., & Bramich, D.M. 2003, *MNRAS*, 344, 527
- Lahav, O., Naim, A., Buta, R.J., Corwin, H.G., de Vaucouleurs, G., et al. 1995, *Science*, 267, 859
- Laurikainen, E., Salo, H., & Buta, R., 2005, *MNRAS*, 362, 1319
- Laurikainen, E., Salo, H., Buta, R., & Knapen, J. 2007, *MNRAS*, 381, 401
- Laurikainen, E., Salo, H., Buta, R., Knapen, J., Speltincox, T., & Block, D., 2006, *AJ*, 132, 2634
- Leeuw, L.L., Davidson, J., Dowell, C.D., Matthews, H.E. 2008, *ApJ*, 677, 249
- Lintott, C.J., et al. 2008, *MNRAS*, submitted (arXiv:0804.4483)
- Liu, F.S., Xia, X.Y., Mao, S., Wu, H., Deng, Z.G. 2008, *MNRAS*, 385, 23
- Longmore, A.J., Hawarden, T.G., Goss, W.M., Mebold, U., & Webster, B.L. 1982, *MNRAS*, 200, 325
- Loveday, J., 1996, *MNRAS*, 278, 1025
- MacArthur, L.A., Courteau, S., & Holtzman, J.A., 2003, *ApJ*, 582, 689
- Maller, A.H., Berlind, A.A., Blanton, M.R., Hogg, D.W. 2008, *ApJ*, submitted (arXiv:0801.3286)
- Márquez, I., Lima Neto, G.B., Capelato, H., Durret, F., Lanzoni, B., & Gerbal, D. 2001, *A&A*, 379, 767
- Masters K. L., Giovanelli R., Haynes M. P., 2003, *AJ*, 126, 158
- Mathis, H., Lemson, G., Springel, V., Kauffmann, G., White, S.D.M., Eldar, A., & Dekel, A. 2002, *MNRAS*, 333, 739
- Mayer, L., Governato, F., Kaufmann, T. 2008, *Advanced Science Letters* (arXiv:0801.3845)
- Meisels, A., & Ostriker, J. P. 1984, *AJ*, 89, 1451
- Méndez-Abreu, J., Aguerri, J.A.L., Corsini, E.M., Simonneau, E. 2008, *A&A*, submitted (arXiv:0710.5466)
- Merritt, D., Graham, A.W., Moore, B., Diemand, J., & Terzić, B. 2006, *AJ*, 132, 2685
- Mo, H.J., Mao, S., White, S.D.M. 1998, *MNRAS*, 295, 319
- Möllenhoff, C. 2004, *A&A*, 415, 63
- Möllenhoff, C., & Heidt, J. 2001, *A&A*, 368, 16

- Möllenhoff, C., Popescu, C.C., & Tuffs, R.J. 2006, *A&A*, 456, 941
- Navarro, J.F., & Benz, W. 1991, *ApJ*, 380, 320
- Navarro, J.F., & White, W. 1994, *MNRAS*, 267, 401
- Nipoti, C., Londrillo, P., & Ciotti, L. 2006, *MNRAS*, 370, 681
- Okamoto, T., Eke, V. R., Frenk, C. S., & Jenkins, A. 2005, *MNRAS*, 363, 1299
- Ostriker, J. P. 1977, *Proceedings of the National Academy of Science*, 74, 1767
- Padilla, N.D., Strauss, M.A. 2008, *MNRAS*, submitted (arXiv:0802.0877)
- Patterson, F.S., 1940, *Harvard College Observatory Bulletin*, 914, 9
- Peletier, R.F., & Balcells, M. 1996, *AJ*, 111, 2238
- Peletier, R.F. & Willner, S.P. 1992, *AJ*, 103, 1761
- Popescu, C.C., Misiriotis, A., Kylafis, N.D., Tuffs, R.J., & Fischera, J. 2000, *A&A*, 362, 138
- Popescu, C.C. et al. 2005, *ApJ*, 619, L75
- Popescu, C.C., & Tuffs, R.J. 2007, in *Proceedings of the lectures given at the Les Houches Winter School "Astronomy in the submillimeter and far infrared domains with the Herschel Space Observatory"* (arXiv:0709.2310)
- Press, W.H., Teukolsky, S.A., Vetterling, W.T., & Flannery, B.P., 1992, *Numerical recipes* (2nd ed.; Cambridge: Cambridge Univ. Press)
- Prieto, M., Aguerri, J.A.L., Varela, A.M., & Muñoz-Tuñon, C. 2001, *A&A*, 367, 405
- Prugniel, P., & Simien, F. 1997, *A&A*, 321, 111
- Scannapieco, C., & Tissera, P.B. 2003, *MNRAS*, 338, 880
- Reese, A.S., Williams, T.B., Sellwood, J.A., Barnes, E.I., & Powell, B.A. 2007, *AJ*, 133, 2846
- Reichard, T.A., Heckman, T.M., Rudnick, G., Brinchmann, J., Kauffmann, G. 2008, *ApJ*, 677, 186
- Rest, A., et al. 2001, *AJ*, 121, 2431
- Rix, H.-W., & Zaritsky, D. 1995, *ApJ*, 447, 82
- Sadler, E. M., & Gerhard, O. E. 1985, *MNRAS*, 214, 177
- Sandage, A. 1961, *The Hubble Atlas of Galaxies* (Washington: Carnegie Inst. Washington)
- Satyapal, S., Vega, D., Dudik, R. P., Abel, N. P., & Heckman, T. 2008, *ApJ*, 677, 906
- Satyapal, S., Vega, D., Heckman, T., O'Halloran, B., & Dudik, R. 2007, *ApJ*, 663, L9
- Scannapieco, C., Tissera, P. B., White, S. D. M., & Springel, V. 2008, *MNRAS*, submitted (arXiv:0804.3795)
- Schlegel, D. J., Finkbeiner, D. P., & Davis, M. 1998, *ApJ*, 500, 525
- Seigar, M.S., Graham, A.W., Jerjen, H. 2007, *MNRAS*, 378, 1575
- Seigar, M.S., & James, P.A. 1998, *MNRAS*, 299, 672
- Sérsic, J.-L. 1963, *Boletín de la Asociación Argentina de Astronomía*, vol.6, p.41
- Sérsic, J.-L. 1968, *Atlas de Galaxias Australes* (Cordoba: Observatorio Astronomico)
- Shao, Z., Xiao, Q., Shen, S., Mo, H. J., Xia, X., & Deng, Z. 2007, *ApJ*, 659, 1159
- Shen, S., Mo, H. J., White, S. D. M., Blanton, M. R., Kauffmann, G., Voges, W., Brinkmann, J., & Csabai, I. 2003, *MNRAS*, 343, 978
- Shields, J.C., Walcher, C.J., Boeker, T., Ho, L.C., Rix, H.-W., van der Marel, R.P. 2008, *ApJ*, in press (arXiv:0804.4024)
- Simien, F., & de Vaucouleurs, G. 1986, *ApJ*, 302, 564
- Smith Castelli, A.V., Bassino, L.P., Richtler, T., Cellone, S.A., Aruta, C., Infante, L. 2008, *MNRAS*, in press (arXiv:0803.1630)
- Springel, V., Di Matteo, T., & Hernquist, L. 2005a, *MNRAS*, 361, 776
- Springel, V., Di Matteo, T., & Hernquist, L. 2005b, *ApJ*, 620, L79
- Springel, V., White, S.D.M., Tormen, G., & Kauffmann, G. 2001, *MNRAS*, 328, 726
- Springel, V., & Hernquist, L. 2003, *MNRAS*, 339, 289
- Steinmetz, M., & Navarro, J. F. 2002, *New Astronomy*, 7, 155
- Temì, P., Brighenti, F., & Mathews, W.G., 2007, *ApJ*, 660, 1215
- Terzić, B., & Graham, A.W. 2005, *MNRAS*, 362, 197
- Terzić, B., & Sprague, B.J. 2007, *MNRAS*, 377, 855
- Tonry, J.L., et al., 2001, *ApJ*, 546, 681
- Trujillo, I., Asensio Ramos, A., Rubiño-Martín, J. A., Graham, A. W., Aguerri, J. A. L., Cepa, J., & Gutiérrez, C. M. 2002, *MNRAS*, 333, 510
- Trujillo, I., Graham, A.W., & Caon, N. 2001, *MNRAS*, 326, 869
- Tuffs, R. J., Popescu, C. C., Völk, H. J., Kylafis, N. D., & Dopita, M. A. 2004, *A&A*, 419, 821
- Tully, R. B., Pierce, M. J., Huang, J.-S., Saunders, W., Verheijen, M. A. W., & Witchalls, P. L. 1998, *Aj*, 115, 2264
- Untertorn, C.T., & Ryden, B.S. 2008, *ApJ*, submitted (arXiv:0801.2400)
- Valentijn, E.A. 1990, *Nature*, 346, 153
- van den Bosch F.C. 2001, *MNRAS*, 327, 1334
- van Leeuwen, F., Feast, M.W., Whitelock, P.A., & Laney, C.D. 2007, *MNRAS*, in press (arXiv:0705.1592)
- Weinzirl, T., Jøgee, S., Barazza, F.D. 2008, (arXiv:0802.3903)
- Whitford, A. E. 1958, *AJ*, 63, 201
- Xilouris E.M., Byun Y.I., Kylafis N.D., Paleologou E.V., Papanastorakis J., 1999, *A&A*, 344, 868
- York, D.G., et al. 2000, *AJ*, 120, 1579
- Yoshizawa, M., & Wakamatsu, K. 1975, *A&A*, 44, 363
- Young, C. K., & Currie, M. J. 1994, *MNRAS*, 268, L11